



5-2005

Modeling and Simulation of a Trailer with Band Track over Wheels

Hemmant Gopal

University of Tennessee - Knoxville

Follow this and additional works at: https://trace.tennessee.edu/utk_gradthes



Part of the [Mechanical Engineering Commons](#)

Recommended Citation

Gopal, Hemmant, "Modeling and Simulation of a Trailer with Band Track over Wheels. " Master's Thesis, University of Tennessee, 2005.

https://trace.tennessee.edu/utk_gradthes/1919

This Thesis is brought to you for free and open access by the Graduate School at TRACE: Tennessee Research and Creative Exchange. It has been accepted for inclusion in Masters Theses by an authorized administrator of TRACE: Tennessee Research and Creative Exchange. For more information, please contact trace@utk.edu.

To the Graduate Council:

I am submitting herewith a thesis written by Hemmant Gopal entitled "Modeling and Simulation of a Trailer with Band Track over Wheels." I have examined the final electronic copy of this thesis for form and content and recommend that it be accepted in partial fulfillment of the requirements for the degree of Master of Science, with a major in Mechanical Engineering.

Jeffrey S. Freeman, Major Professor

We have read this thesis and recommend its acceptance:

J. A. M. Boulet, William R. Hamel

Accepted for the Council:

Carolyn R. Hodges

Vice Provost and Dean of the Graduate School

(Original signatures are on file with official student records.)

To the Graduate Council:

I am submitting herewith a thesis written by Hemmant Gopal entitled “Modeling and Simulation of a Trailer with Band Track over Wheels”. I have examined the final copy of this thesis for form and content and recommend that it be accepted in partial fulfillment of the requirements for the degree of Master of Science, with a major in Mechanical Engineering.

Jeffrey S. Freeman

Major Professor

We have read this thesis
and recommend its acceptance:

J. A. M. Boulet

William R. Hamel

Accepted for the Council:

Anne Mayhew

Vice Chancellor and Dean of Graduate Studies

(Original signature are on file with official students records)

MODELING AND SIMULATION OF A TRAILER WITH BAND TRACK OVER WHEELS

A Thesis
presented for the
Master of Science Degree
The University Of Tennessee, Knoxville

Hemmant Gopal
May 2005

Acknowledgments

This thesis would never have seen the light of day, if not for the immense help provided by a few people.

I would take the time to thank Dr. Jeffrey S. Freeman, my advisor and guide, who gave me the opportunity to work on this thesis and has stood by me through this effort, without whose support and constant guidance, I would still be on square one . Even through his busy schedule, he found the time to answer my questions and point me in the right direction.

I would like to thank Dr. J. A. M. Boulet and Dr. William R. Hamel to have agreed to be on my thesis committee.

I would like to thank Anandha Gopalan, my brother, who has always lent me an ear when I needed to rave and rant about my work. I would also like to thank my friends for their never ending support.

Contents

1	Introduction	1
1.1	Background	2
1.2	Objectives	3
1.3	Scope	3
1.4	Thesis overview	4
2	Literature review	6
2.1	Tire models from the literature	6
2.1.1	Simple tire models	6
2.1.2	Linear radial spring tire model	8
2.1.3	Quadratic radial spring tire model	9
2.1.4	Radial-interradial spring tire model	10
2.2	Track models	11
2.2.1	Approaches to modeling	12
2.2.2	Mettalic tracks	13
2.2.3	Elastic band tracks	19
3	Terrain	22
3.1	Soils	22
3.1.1	Soil bearing capacity	23
3.2	Terrain	23
3.2.1	Beviameter test in homogenous and non-homogenous soils . . .	24
3.2.2	Cone penetrometer	27

3.2.3	Penetrometer vs Bevameter	29
3.3	Model used in the research	30
4	Vehicle model	32
4.1	Tracked vehicle model	32
4.2	Formulation of the model	33
4.2.1	Position analysis	33
4.2.2	Velocity analysis	35
4.2.3	Acceleration analysis	37
4.2.4	Joint formulation	37
4.3	Dynamic formulation of the vehicle model	42
4.4	External forces	44
4.4.1	Translational spring damper actuators	44
4.4.2	Rotational spring damper actuator	46
4.5	The layout and algorithm for the current model	47
5	Track model	50
5.1	Model description	50
5.2	Location of the radial springs, calculation of tire deflections and tire forces	52
5.3	Track connectivity algorithm	56
5.4	Forces generated by track terrain interaction	59
5.5	Track tension	61
5.6	The algorithm	64
6	Results	66
6.1	Test of trailer model without the track model	66
6.1.1	Conclusions	71
6.2	Performance at different speeds	71
6.2.1	Test of track model- sandy loam	71
6.2.2	Test of track model- sand	77

6.3	Soil performance	83
6.4	Performance on rough terrain	87
7	Conclusions and future work	90
7.1	Conclusions	90
7.2	Future work	92
	Bibliography	94
	Vita	97

List of Tables

3.1	Main trafficability features of friction and cohesion soils[11]	23
6.1	Theoretical shear vs Actual shear	83
6.2	Theoretical sinkage vs Actual sinkage	85

List of Figures

1.1	M200 trailer	3
2.1	Point contact model[4]	7
2.2	Rigid tread band tire model[4]	7
2.3	Fixed foot print model[4]	7
2.4	Radial spring tire model [4]	9
2.5	Radial-interradial tire radial model[4]	10
2.6	The chassis subsystem [12]	13
2.7	Track subsystem [12]	14
2.8	Finite element analysis [10]	15
2.9	Forces acting on track	16
2.10	Shear displacement in forward motion [5]	17
2.11	In plane model representation of high-mobility tracked vehicle [2]	18
2.12	Force consideration of track sag [2]	18
2.13	Track connectivity [2]	19
2.14	Trackpost[3]	20
2.15	Track segments[3]	21
3.1	A model of a bevameter[9]	25
3.2	Pressure under the tire[7]	28
3.3	Cone penetrometer[9]	28
4.1	Revolute joint[1]	38
4.2	Translation joint[1]	41
4.3	Translation spring damper actuators[1]	45

4.4	Rotational spring damper actuator[1]	47
4.5	Layout of the vehicle	48
5.1	Tire deflection	53
5.2	Ground profile	54
5.3	Bump between the wheels	57
5.4	Tire on top of bump	58
5.5	Track elements	61
5.6	Torque around the wheels	63
6.1	Vertical position of frame(dropped)	67
6.2	Vertical position of axle(dropped)	67
6.3	Length of translation joint(dropped)	68
6.4	Vertical position of frame(1m/s)	69
6.5	Horizontal position of axle(1m/s)	69
6.6	Vertical position of frame(10m/s)	70
6.7	Horizontal position of axle(10m/s)	70
6.8	Vertical position of frame(sandy)	72
6.9	Vertical position of the walking beam and tires(sandy)	73
6.10	Angle of the walking beam(sandy)	74
6.11	Rotaional velocity of the wheels(sandy)	75
6.12	Length of translation joint(sandy)	76
6.13	Vertical position of frame(sand)	78
6.14	Vertical position of all bodies(sand)	79
6.15	Angle of the walking beam(sand)	80
6.16	Rotaional velocity of the wheels(sand)	81
6.17	Length of translation joint(sand)	82
6.18	Comparative results between three different soils	84
6.19	Shear force under the tires	84
6.20	Shape of track(sandy)	85
6.21	Shape of track(sand)	85

6.22	Actual shear force	86
6.23	Bar graph of theoretical and actual shear	86
6.24	Vertical position of frame(1m/s)	87
6.25	Vertical position of frame(10m/s)	88
6.26	Vertical position of all bodies(1m/s)	88
6.27	Vertical position of all bodies(10m/s)	89

Chapter 1

Introduction

Terramechanics is a discipline which studies the performance of a vehicle in relation to the terrain characteristics. Terrain-Vehicle mechanics is a branch of terramechanics and deals with the tractive performance of vehicle over unprepared terrain and various obstacles. Over the years terrain models have evolved to include more and more factors, which in turn has helped in modelling the vehicle terrain interaction better and calculate the dynamic forces more accurately.

The various performance characteristics like tractive effort, motion resistance and drawbar pull are determined by the shear and normal stresses on the vehicle at the point where it is in contact with the terrain. The main issue in the modeling off-road vehicles is to predict the vehicle-terrain interaction.

In case of the trailer this is the track-terrain interaction. A model of this interaction leads to a better understanding of the forces on the vehicle in various situations. This helps us diagnose and problems and suggest design changes.

There have been many track models suggested, most dealing with metal tracks. The wheels in these models have been modeled as rigid bodies. There is no complete Track model that can stand by itself independent of the vehicle. This report lists out the concepts behind creating an independent track model that takes the deformation of rubber tires into consideration.

1.1 Background

An extensive survey of literature on the field of off road vehicles has been done. Some of the models are discussed in detail, especially with regard to the track model and track terrain interaction. A complete description of the vehicle model being used is also presented. The methodology of modeling the vehicle is described in detail. A lumped mass model of the track is created and implemented in this study. A set of tests are simulated for the vehicle under different conditions. The simulated results are compared with results from the literature. Since there are no detailed test results available for the actual trailer the model is run through many simulations and the results are verified to see whether they are what would be accepted as reasonable values for a vehicle of its kind.

The model will be used to characterize the performance of the vehicle in following criteria:

1. Performance at different speeds
2. Soil performance
3. Rough terrain performance

The Vehicle

The vehicle that is modeled here is the M200 trailer shown in Figure 1.1. This trailer is designed to carry a 2-ton load . The trailer is most often used to carry generators. A particular configuration is used to carry the Miclic system. Due to the trailer facing difficulties in the field, the trailer was modified from a single-axle 2-wheeled trailer to a single-axle 4-wheeled trailer. A walking beam was welded at both ends of the bogey axle, wheels were attached at the ends of the walking beam and a make shift rubber band track was wrapped around the wheels. Since the whole operation was done in the field there is no technical data package available for the modification. Some of the technical data like the initial track tension and the stiffness of the track are taken from comparable vehicles.



Figure 1.1: M200 trailer

The Miclic system is anti-mine system that consist of rocket that fires a line of cord lined with C4 explosives that are detonated in a mine field. The trailers that carried this configuration had problems related to vehicle sinkage in the desert; due to this the vehicles were modified with a walking beam and band track such that the mean maximum ground pressure was reduced.

1.2 Objectives

The objective of this thesis is to model the U.S army M200 trailer for application in future durability/reliability studies.

1.3 Scope

1. Formulate models for the elastic track, radial spring tyre, multibody dynamics of the vehicle

2. To implement a general trailer model for a elastic rubber track over wheels in Matlab.
3. Verify performance on soil.

1.4 Thesis overview

Chapter 2 Presents a review of the literature. Several different track models are discussed. Formulations, track connectivity and terrain models are investigated. Methods of modeling tires are detailed.

Chapter 3 Different kinds of soils and modeling methods are described. Various models of terrain presentation are discussed. The principles and experiments done to calculate the various parameters are given. Bekker's equations and Janosi and Hanamoto's approximations are discussed in detail.

Chapter 4 The M200 trailer model is discussed in this chapter. The basics of recursive multibody dynamics are mentioned. The analysis of body position, velocity and acceleration are presented. The various joint formulations are detailed. The dynamic analysis of the multibody trailer model is also presented.

Chapter 5 The lumped mass track model is presented in this chapter. The track terrain interactions and the corresponding forces are discussed. The sinkage, pressure distribution under the track, the normal force, shear displacement, shear force, track tension and friction forces are analyzed. The tire force and its effect on the track and vehicle are also described.

Chapter 6 Simulations results are run for different kinds of soils and speeds are presented. These simulations help to understand the effect of the terrain geometry,

vehicle speed and soil type. Due to lack of any test data the model cannot be validated it can only be verified .

Chapter 7 The various advantages of the model are discusses and conclusions are drawn.

Chapter 2

Literature review

2.1 Tire models from the literature

There are many tire models that have been proposed in the past, here a few of them are discussed in detail. Most of these models are an extension of a previous model.

2.1.1 Simple tire models

The first model is the simplest model for tires; point contact model[6]. The point contact model is possibly the most commonly used tire model, it is mathematically represented by a spring and a damper in parallel as shown in Figure 2.1 this results in a fairly good model to calculate the tire forces when tire runs over smooth, long wave length bumps. Its accuracy decreases for rough terrain.

The rigid tread band tire model[6] also follows the same spring and damper model as the point contact, but is mounted on a rigid wheel as shown in Figure 2.2, it experiences a forcing function when the wheel moves. In this model the contact point is not constrained to be vertically below the axle, it can move forward and backward due to encounters with local geometry. This model filters out small wavelength bumps.

The fixed footprint model uses distributed springs and dampers to form the contact model as shown in Figure 2.3. The footprint in the model is constant in size, and

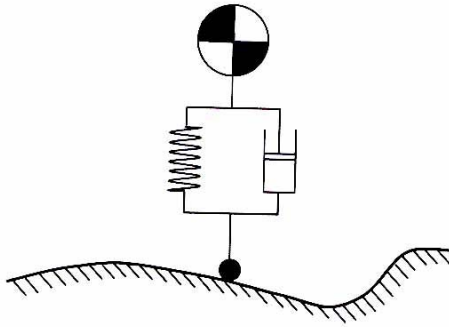


Figure 2.1: Point contact model[4]

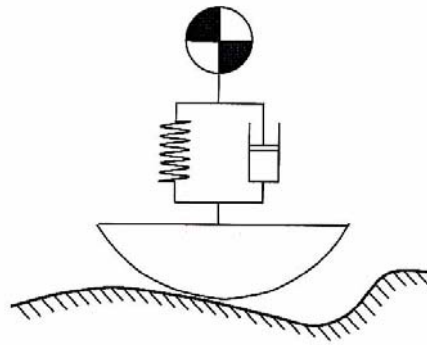


Figure 2.2: Rigid tread band tire model[4]

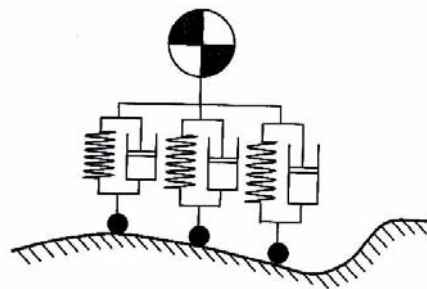


Figure 2.3: Fixed foot print model[4]

independent of the tire deflection. Drag forces for the above models are predicted by assuming that the resultant tire force is always normal to the local ground profile.

2.1.2 Linear radial spring tire model

To overcome the deficiencies of the point contact model the radial spring model was suggested. It uses angularly distributed, independent, linear spring elements as shown in Figure 2.4 [6]. This model has the capability of accurately simulating the tire envelopment of small surface irregularities. It accurately predicts the tire forces over long wave length ground profiles. This tire model suits are needs for the simulation and was used in this research.

The mathematical formulation for this model is as follows,

$$\frac{R - Z}{R - X_j} = \cos\Theta_j \quad (2.1)$$

$$X_j \cos\Theta_j = R(\cos\Theta_j - 1) + Z - Z_w \quad (2.2)$$

$$F_{vj} = K X_j \cos\Theta_j \quad (2.3)$$

$$F_{hj} = F_{vj} * \tan\Theta_j \quad (2.4)$$

$$F_v = \sum_{j=1}^n F_{vj} \quad (2.5)$$

Where Z_w is the vertical displacement of the wheel, X_j is the linear displacement of the element, F_{vj} , F_{hj} are the vertical and horizontal forces due to element j and Z is the height of the bump.

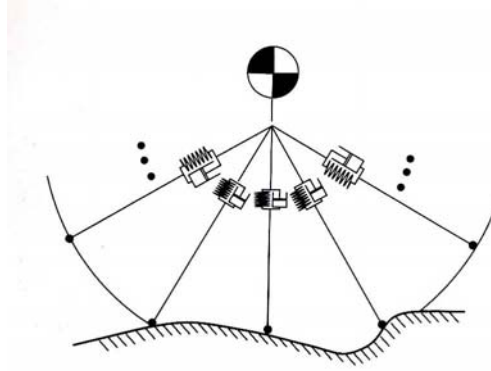


Figure 2.4: Radial spring tire model [4]

2.1.3 Quadratic radial spring tire model

Quadratic radial spring tire model was suggested by Phillips and Cook [4]. This uses radial quadratic spring elements to better approximate the non-linear load deflection curve for a given tire. This model assumes that springs can deflect independent of each other. Only elements in contact with the obstacles are affected; the elements that are not in contact are fully extended to the radius of the tire.

$$F_{rj} = D_1 E_{rj} + D_2 E_{rj}^2 \quad (2.6)$$

The vertical component of force on flat ground in the element j is

$$F_{vj} = F_{rj} \sin \Theta_i \quad (2.7)$$

Where D_1 is the linear spring constant, D_2 is the quadratic spring constant, F_{rj} radial force on tire element j F_{vj} is the vertical force component due to tire element j

The total vertical force is calculated by summing the vertical force due to each tire element, is equal to

$$F_v = \sum_{j=1}^N F_{vj} \quad (2.8)$$

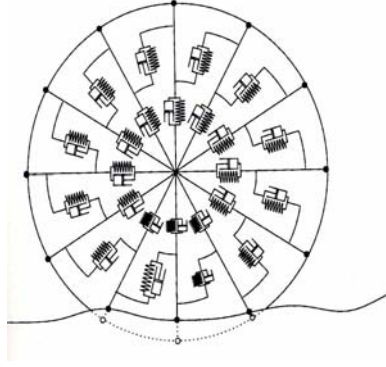


Figure 2.5: Radial-interradial tire radial model[4]

The total drag force can be calculated using the relation

$$F_d = \sum_{j=1}^N F_{vi}/\tan\Theta_j \quad (2.9)$$

2.1.4 Radial-interradial spring tire model

In this model shown in Figure 2.5 there are interradiial springs that connect adjacent radial springs, thereby making the deflection of a particular element dependent on the deflection of its neighboring elements. This predicts more accurately the vertical and drag forces when the tire is not completely supported by the ground or is in contact with an obstacle. Two types of radial models were proposed, linear radial-linear interradiial model and the quadratic radial-linear interradiial spring model[4].

The mathematical models for both the models are as follows

Linear radial-Linear interradiial spring tire model

The radial force on element j is as follows

$$F_{rj} = C_1 E_{rj} + k(2E_{rj} - E_{rj-1} - E_{rj+1}) \quad i = 2, 3, \dots, n - 1 \quad (2.10)$$

$$F_{r1} = C_1 E_{r1} + k(E_{r1} - E_{r2}) \quad (2.11)$$

$$F_{rn} = C_1 E_{rn} + k(E_{rn} - E_{rn-1}) \quad (2.12)$$

$$F_v = \sum_{j=2}^{n-2} [F_{rj} \sin \Theta_j] + F_{r1} \sin \Theta_1 + F_{rn} \sin \Theta_n \quad (2.13)$$

Where C_1 is the linear spring constant, F_{rj} radial force on tire element j F_{vj} is the vertical force component due to tire element j . E_{rj} is the radial displacement of the tire element. c_1 and k must be determined from a tire deflection curve and two simultaneous equations.

Quadratic Radial-Linear Interradial tire model

The radial force in element j is

$$F_{rj} = C_1 E_{rj} + C_2 E_{rj}^2 + k(2E_{rj} - E_{rj-1} - E_{rj+1}) \quad i = 2, 3, \dots, n - 1 \quad (2.14)$$

$$F_{r1} = C_1 E_{r1} + C_2 E_{r1}^2 + k(E_{r1} - E_{r2}) \quad (2.15)$$

$$F_{rn} = C_1 E_{rn} + C_2 E_{rn}^2 + k(E_{rn} - E_{rn-1}) \quad (2.16)$$

$$F_v = \sum_{j=2}^{n-2} [F_{rj} \sin \Theta_j] + F_{r1} \sin \Theta_1 + F_{rn} \sin \Theta_n \quad (2.17)$$

Where C_1 is the linear spring constant, C_2 is the quadratic spring constant, and F_{rj} is the radial force on tire element j . F_{vj} is the vertical force component due to tire element j . C_1, C_2 and k must be determined from a tire force deflection curve and 3 simultaneous equations.

2.2 Track models

There are many individuals and groups of people doing research on tracked vehicles. A large collection of papers on the subject of tracks and track-terrain interaction exists. In this section some of those papers will be investigated.

2.2.1 Approaches to modeling

J.Y.Wong[8] wrote a paper about terramechanics, in which he discusses the measurement of various parameters of the soil using the cone penetrometer and bevameter techniques. The paper also discusses the various methods of approach to terramechanics. These methods are:

1. Empirical approach

This method came into being to circumvent the difficulty in modeling the interaction between an off-road machine and the terrain. Vehicles are tested in on various different types of soils, the soil parameters are also calculated using simple measurements. The values are then empirically correlated. This gives us a scale between the two parameters. Nowadays this method is used to empirically correlate some performance parameters of tires with mobility numbers based on the cone index. This method has had some success but cannot work for certain type of sands, the empirical relationship is valid only within a specific range for which it was tested. Thereby extrapolation of the relationship need not be valid.

2. Theoretical approach

The theory of plastic equilibrium is applied to the soil, this generally provides a good insight into the physical nature of the machine-terrain interaction and can establish a theoretical reference with which performance of off-road vehicles can be compared under ideal conditions. There are some limitations to the application of the theoretical method for prediction of performance of vehicles. The theory of plastic equilibrium is based on the assumption that the terrain behaves like a rigid plastic material, the terrain does not deform much till the stress it reaches a point where failure occurs, beyond this point the strain increase rapidly while the stress remains constant. Most terrains do not display this property. The theory of plastic equilibrium is mainly concerned with the prediction of the load that will cause failure of soil, it does not really deal with deformation of soil under load.

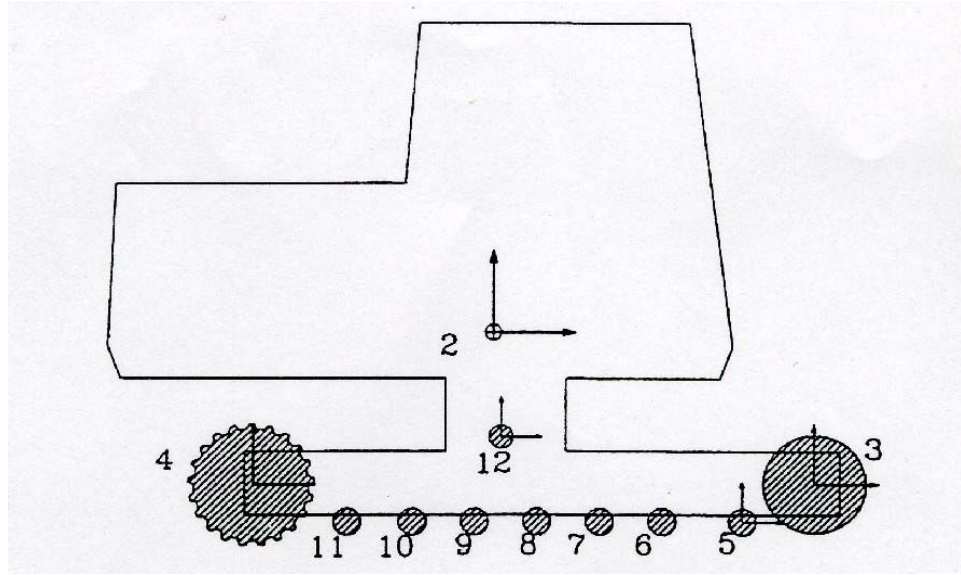


Figure 2.6: The chassis subsystem [12]

3. Semi-empirical approach

Many different semi-empirical methods for predicting off-road performance have been proposed, the most commonly used of them is based on the bevameter technique. In this model terrain characteristics like pressure-sinkage relationship, shear strength and response to repetitive loading obtained using the bevameter technique, are used as inputs. Vehicle parameters like weight, track dimension, track tension, and road wheel arrangement and dimension, are taken into account. The normal and shear stress distributions, normal pressure and motion resistance are the outputs from this model. This is the approach followed for calculation of the parameters in this particular model.

2.2.2 Metallic tracks

Nakanishi and Shabana[12] modeled a hydraulic excavator tracked vehicle as shown in Figure 2.6. The vehicle is modeled as two kinematically decoupled systems, having a total of fifty five degrees of freedom. The track is modeled as a closed kinematic chain that consist of fifty four rigid links connected by revolute joints as shown in

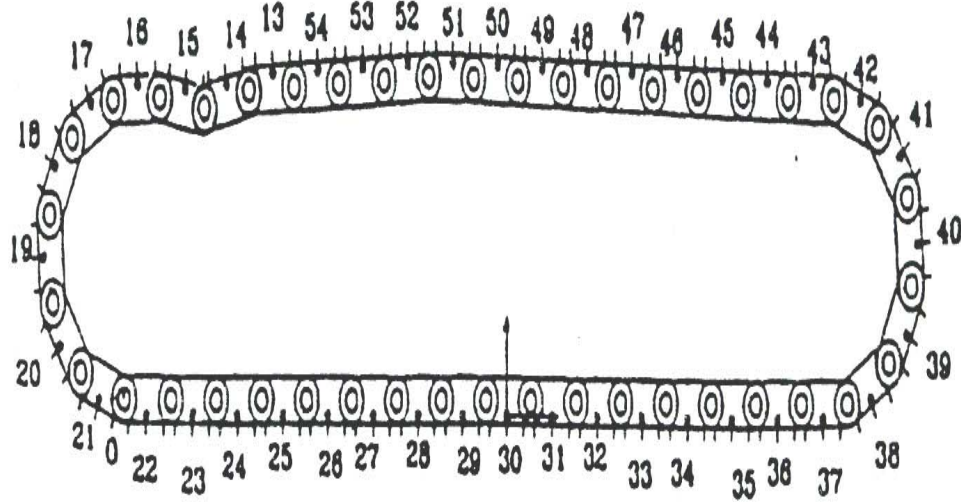


Figure 2.7: Track subsystem [12]

Figure 2.7. The track has forty two degrees of freedom. To define the track configuration in global coordinate system, the author choose two translation cartesian coordinates, the other forty coordinates are chosen as rotational angles. Dependent coordinates are expressed in terms of the independent angles using the described loop closure equations. The dependent velocities and accelerations are calculated in terms of the independent variables by the differentiating the loop equation, these in turn has been used to calculate the velocity and acceleration equations for the track links.

The solution for the nonlinear dynamics for the multi-body equations are obtained by the authors, using two different methods. The methods are described below

The first method is based on the principle of formulating nonlinear algebraic equations are adjoined to the differential equations using the technique of legrange multipliers. The independent coordinates of the tracked vehicle are identified and the associated state equations are integrated for the independent joints and velocities. Iterative Newton-Raphson algorithm is used to solve the constraint equations.

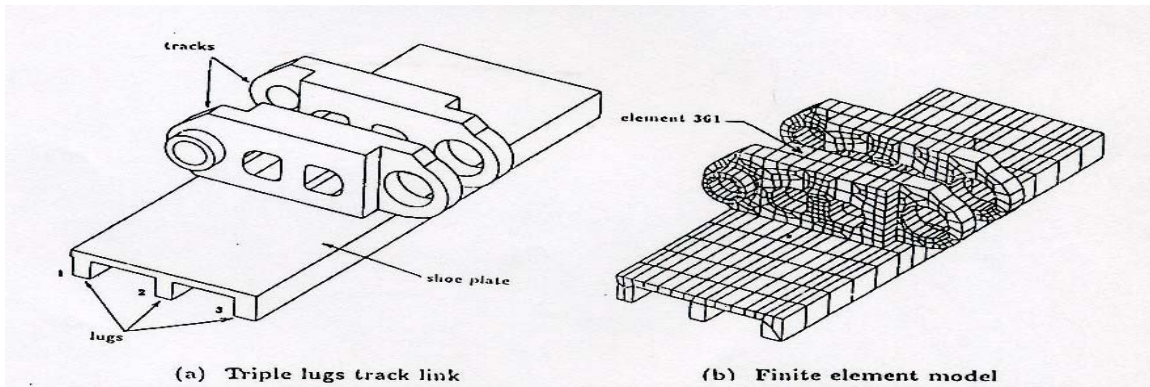


Figure 2.8: Finite element analysis [10]

In the second method in order to avoid the use of Newton-Raphson algorithm in solving the mixed system of differential and algebraic equations of motion, a velocity transformation method is used. The dependent coordinates, velocities are obtained in terms of the independent coordinates.

Both the results agree quiet well, but the second method only uses 54 percent of the cpu time than the first method.

Sarwar, Nakanishi, and Shabana [10] investigated the chain link deformation in the nonlinear dynamics of tracked vehicles. The purpose of the study is to demonstrate the errors that may result from the use of static-force analysis. The track model presented in this paper is the used. In the analysis presented in this paper assumes that the deformation of the steel track links does not have a significant effect on the rigid-body motion of the tracked vehicle. The results of this analysis as shown in Figure 2.8 proves that the dynamic stresses can be significantly different from the static stresses. This is due to the fact that dynamic stress analysis takes into effect the time history of forces.

In their paper about modeling of agricultural vehicles Gianni and Roberto [5], look at the steerability, ride characteristics and prediction of ground pressure distribution

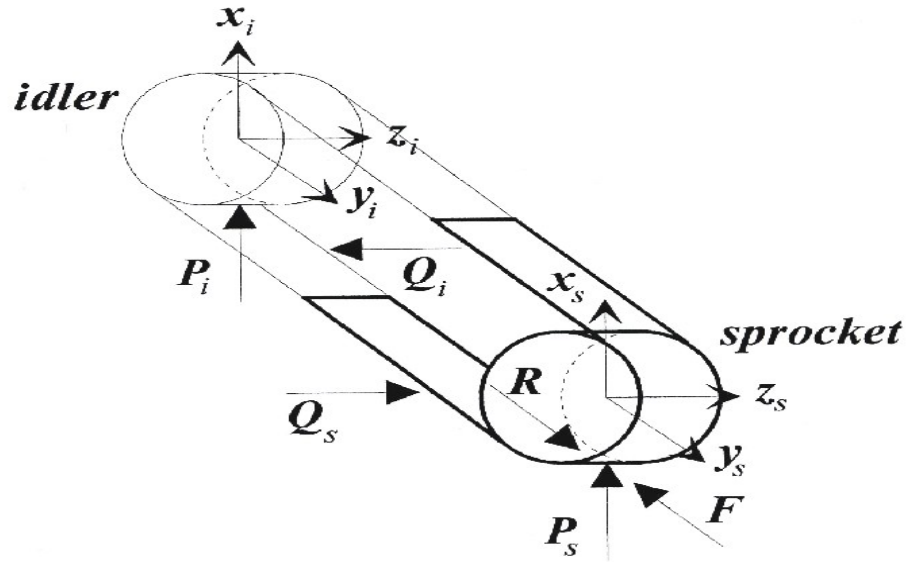


Figure 2.9: Forces acting on track
[5]

an tractive forces. A three dimensional model of the agricultural tracked vehicle is developed which has 8 degrees of freedom and two independently applied sprocket torques as applied input. While looking at steerability the track is assumed to behave as though it were sliding on the ground, the terrain is assumed to be non deformable in the analysis of the vehicle ride characteristics. A two dimensional static model of track-terrain interaction has been developed, as shown in Figure 2.9, the track is divided into four parts an upper run supported by rollers a lower run in contact with the ground and the sections in contact with the idler and the sprocket. The interaction along the track is averaged and the internal forces acting at the pins are ignored, to gain computational efficiency in the numerical solution of the overall model. While calculating the shear stress the track is assumed to be infinitely stiff horizontally, so the track cannot expand, the speed of slip of the track with reference to the ground is is the same for every point of the track in contact with the terrain. The shear displacement under the track is as shown in Figure 2.10. The parameter analysis is based on the bevameter technique proposed by Bekker [9]. The dynamic model gives satisfactory results, however the model to simplified to provide a realistic description

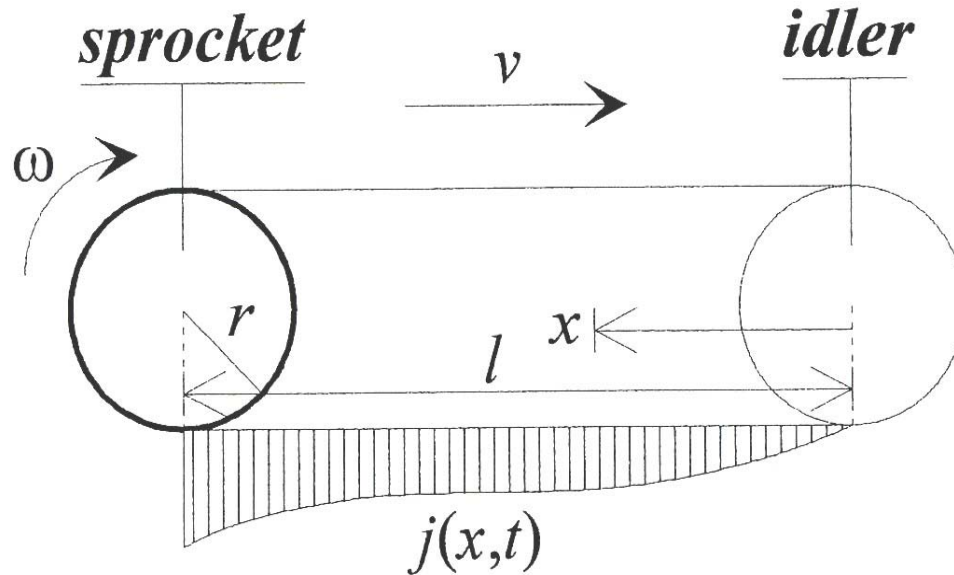


Figure 2.10: Shear displacement in forward motion [5]

of the dynamics of the overall tracked vehicle system.

Dhir and Sankar[2] created a computer simulation model for predicting the dynamics of off-road tracked vehicles. A two-dimensional tracked vehicle model is developed as shown in Figure 2.11, with detailed analytical representation of the trailing arm suspension and dynamic wheel-track-terrain interaction. The wheel-track-terrain interaction is modeled via an improved adaptive footprint formulation. The track is made of steel tracks interconnected with rubber pads of both the inner and outer surfaces. The terrain is assumed to be a non-deformable. The terrain profile is modeled like a set of linear segments adjoining the coordinates of successive points. It is represented by a table containing horizontal and vertical coordinates of successive points, the values of the intermediate points are calculated by linear interpolation. The kinematics of the vehicle model is described by $2+N$ generalized coordinates. The track sag is calculated by using a quadratic polynomial approach, which permits a direct visualization of track sag as shown in Figure 2.12 as a function of track tension. The track connectivity for the track is modeled as shown in Figure 2.13.

The horizontal and vertical forces due to the dynamic vehicle-terrain interaction

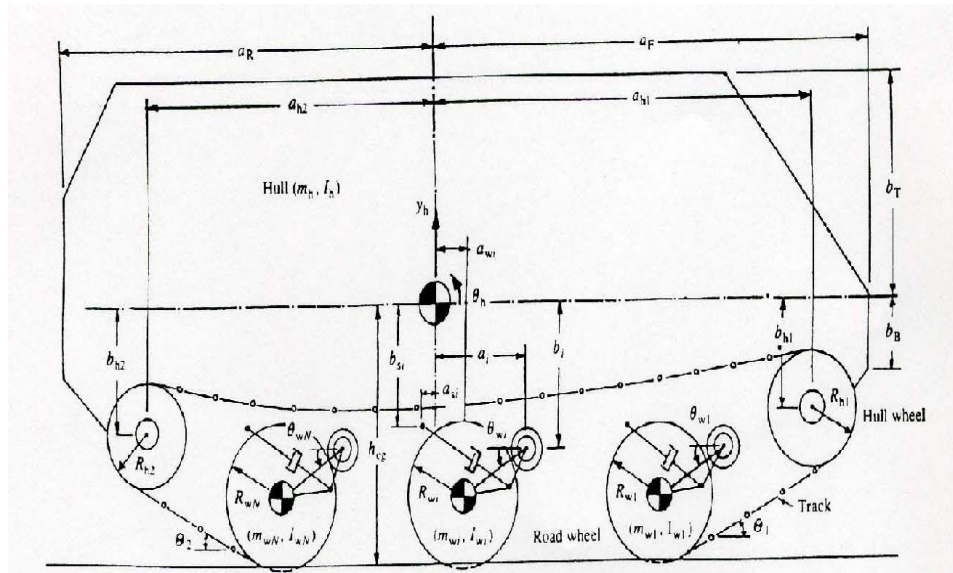


Figure 2.11: In plane model representation of high-mobility tracked vehicle [2]

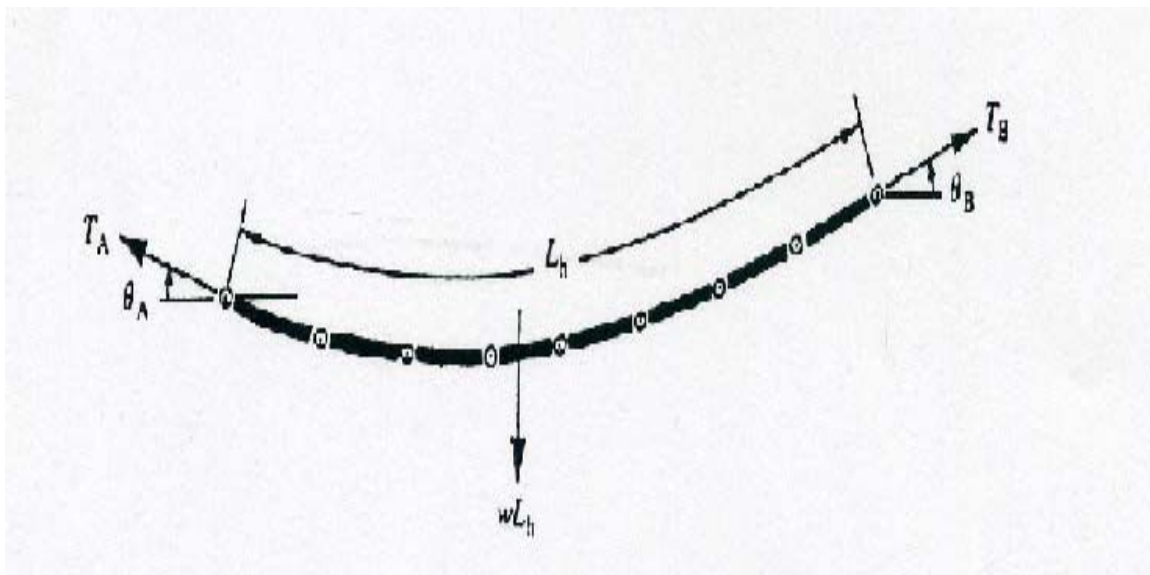


Figure 2.12: Force consideration of track sag [2]

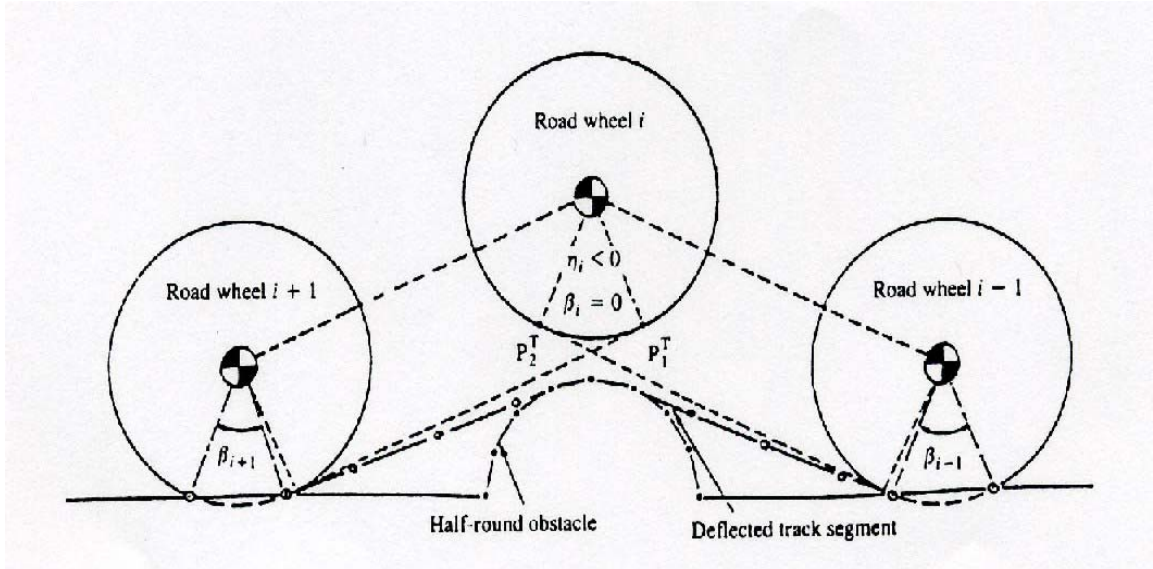


Figure 2.13: Track connectivity [2]

are computed. The suspension forces and moments are computed based on the road arm orientation. The equations of motion are integrated based on hamming's modified predictor-corrector method.

2.2.3 Elastic band tracks

The model that the present research is primarily derived from is based on the thesis by Corina Sandu [3]. In this study the track is modeled as a continuous flexible belt. The band has only longitudinal elasticity and therefore one degree of freedom. This model is used for straight line testing. This model takes into account the moment of inertia of the road wheel and it adds friction force model at the road wheel-track interface. It is a scalar model. The assumptions that are made are that the track doesn't slip on the sprocket, or the idler, the track is quasi static and the track tension acts along the tangent to the wheel at the wheel track separation point. The suspension of each road wheel is modeled using rotational spring dampers. The way the track is modeled there is no shear between the road wheels. The track is modeled as a single force element. The track terrain interaction is modeled in detail, the

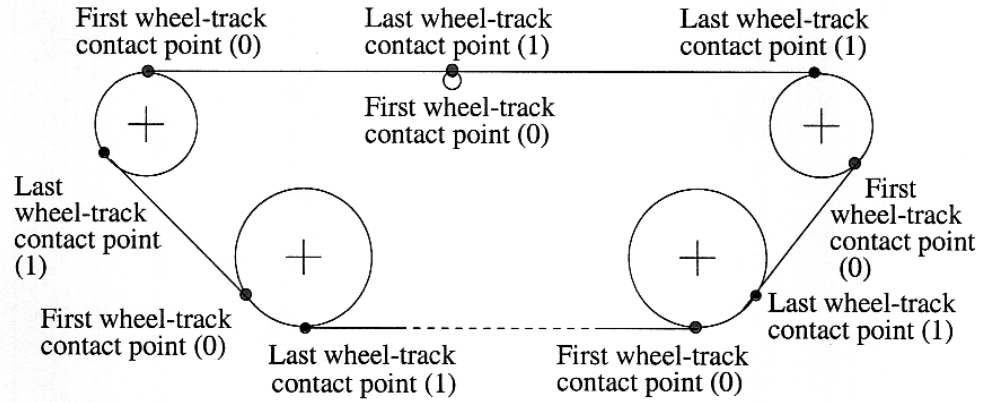


Figure 2.14: Trackpost[3]

vehicle-terrain interaction is modeled using relationships developed by Bekker [9] and Wong [7]. A detailed connectivity algorithm is written, which divides the track into segments as shown in Figure 2.14. The forces on each of the track segments are shown in Figure 2.15.

Connectivity Algorithm

1. Track segment wrapped around the idler
2. Track segment along the common tangent between the first road wheel and idler
3. Track segment around the sprocket
4. Lower portion of the track, in contact with the road wheel and ground.
5. Upper portion of the track segment between the sprocket and the idler

After calculating the track-terrain interaction forces and wheel-track forces the tensions for the whole model are calculated.

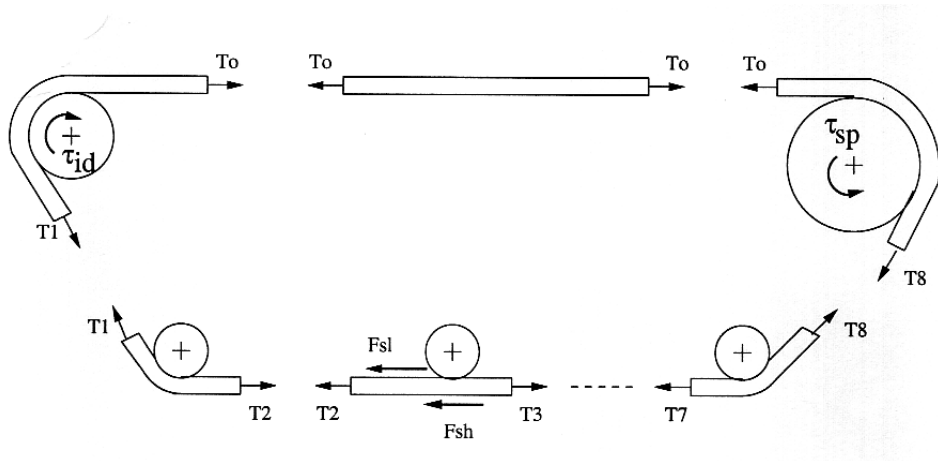


Figure 2.15: Track segments[3]

Chapter 3

Terrain

3.1 Soils

There are various forms of soil. Soils are classified in many different ways to suit different purposes, these are used by different fields like engineering, agricultural ventures and military. The basic classification from a geological perspective is as follows

1. Alluvial soils :- Deep deposits of homogenous soil particles like clay soils and sandy soils
2. Moraine soils :- Mixture of soil particles of different sizes, Moraine soils are often shallow because the rock bottom is near the surface.
3. Organic soil :- Organic terrain consist of a mat of living vegetation on the surface and a layer of saturated peat beneath it.

The soils are also classified from a engineering perspective as friction and cohesion soils. In terramechanics, the main distinction is made between friction and cohesion soils because the typical behavior under the wheel loads differs. The main features of each type are listed in table 3.1

Table 3.1: Main trafficability features of friction and cohesion soils[11]

Friction soil	Cohesion soil
Changes in water content have small variation in trafficability	When wet very poor trafficability, but increases toward drier conditions
Soil density plays a remarkable role in trafficability	Soil moisture plays a remarkable role in trafficability
Trafficability increases under repetitive loading increases upto a certain strength	Trafficability worsens after soil disturbance, and soil have only residual strength

3.1.1 Soil bearing capacity

The soil bearing capacity differs according to the method used to measure it. In the forest, soil bearing capacity is usually considered as the maximal allowable wheel contact pressure. The actual wheel contact pressure however, is difficult to assess because the true contact area depends on tire and soil properties. In the WES method, the soil bearing capacity is linked directly to the soil penetration resistance, and the Cone index can be considered as an indicator of bearing capacity. Soil engineering studies the sinkage of the wheel or track, which in turn is the output of various soil models developed. The input for these soil models vary. Bekker's [9] model uses the concept of flotation as a description of soil bearing capacity. The method is based on the elastic theory, in which the load sinkage relationship is measured using round plates with different diameters. The constants are calculated from the load-sinkage curve.

3.2 Terrain

The evaluation of terrain-vehicle interaction is based on a number of parameters which pertain to both the terrain and the vehicle. Off-road vehicles will have to work in physical environments that contain plants, ice, snow, water, surface soils, natural and artificial static objects etc. Investigation of terrain-vehicle relationships with respect to mechanical efficiency of motion and effectiveness of mission accomplishment led to the usage of mathematical models of terrain. These models involved the physical and

geometrical properties of the terrain. These mathematical models yield definition of design and performance parameters, which in turn lead to optimization of vehicle concept.

The two most commonly used terrain models are based on the cone-penetrometer and bevameter test. During World War II, the Americans and British developed methods to measure the various parameters of the soil. The Americans used a non-recording penetrometer equipped with a conical head to define soil trafficability; resistance to penetration encountered by the cone was empirically correlated with 'go' and 'no go' performance of the vehicle. The British military developed a penetrometer with a circular plate and a recorder to plot the constant rate load-penetration curve for the measured soil. In the early 1950's Dr. Bekker [9] created a mathematical model for the vertical and horizontal stress strain relationship, with the help of data from a bevameter. A common bevameter is shown in Figure 3.1. This mathematical model is still used widely.

3.2.1 Bevameter test in homogenous and non-homogenous soils

Mechanical properties of soil like soil failure are defined by the stress-strain relationships. Due to lack of rigorous and practical solutions for soil failure, only semi-empirical methods have been able to define such relationships for predicting vehicle performance and design parameters. For a successful semi-empirical solution to be created, it is important to make sure that the loading condition of both the vehicle and soil measuring apparatus are as similar as possible. Since the horizontal and vertical loads produced by the vehicle are balanced by the soil thrust and motion resistance, a formulation for the vertical and horizontal stress-strain relation can be calculated from any such model. A bevameter as shown in Figure 3.1, is a suitable device to measure the terrain values.

This type of instrumentation affects the readings quite a bit, the instrument that best simulates vehicle ground contact areas are those with rectangular or annular plates, which shear the terrain under predetermined vertical loads, that correspond to

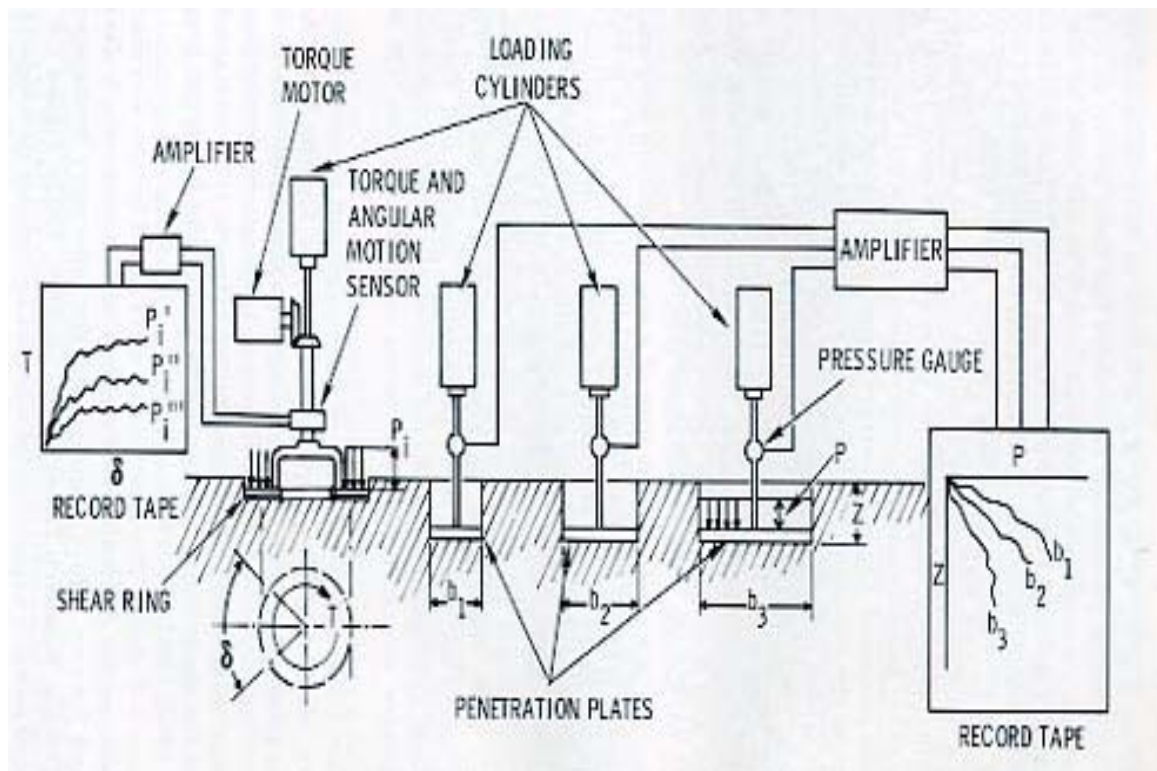


Figure 3.1: A model of a bevameter[9]

the vehicle ground pressure. This technique can be used to determine both the vertical and horizontal stress-strain relationship. The vertical stress strain relationship is described as follows.

An experimentally proven fact [9]; that if a plate penetrates soil to depth z under pressure p then the empirical curve can be fitted with equation

$$p \cong kz^{0.5} \quad (3.1)$$

Where k is the modulus of inelastic deformation and 0.5 is the exponent of sinkage. After numerous tests and computation a more generalized formulation was achieved.

$$p = [(k_c/b) + k_\varphi]z^n \quad (3.2)$$

Where k_c and k_φ are cohesive and frictional moduli of deformation, these are insensitive to plate radius and width. b is the smaller dimension of the loading area. The parameters k_c , k_φ and n can be calculated if two test with 2 different radii are conducted. With a two plate bevameter, each test produces two curves, on a log-log scale they represent the following equations.

$$\ln p_1 = \ln [(k_c/b_1) + k_\varphi] + n \ln z \quad (3.3)$$

$$\ln p_2 = \ln [(k_c/b_2) + k_\varphi] + n \ln z \quad (3.4)$$

From the following equations k_c , k_φ and n can be easily calculated. This formulation, which only works for homogeneous soils, fits most natural conditions, due to the fact that in shallow depth soil behaves as if it were homogeneous. This model fails under certain circumstances. The constants are insensitive to the plate size only if the test plate deforms the soil the same way the vehicle deforms it. In some soils small plate sizes do not deform the soil the way the vehicles do, the other factor in determining the minimum are impurities in the soil and localized density functions. Due to these defects the formulation does not work very well when scaled, therefore cannot be used in analyzing the terrain-vehicle interaction for small robots etc.

The model also calculates the horizontal shear-strain relationship. The horizontal stress strain relationship is based on the coulomb's equation $\tau = (c + p \tan \varphi)$. Where shear stress τ is related to two parameters, cohesion, 'c' and friction 'φ' . The plotting of $\tau(j)$ curves for various normal loads p serves to determine the envelope of Mohr circles based on coulomb's criterion of soil failure. From this envelope we can deduce the values of c and φ .

To account for the slip of the vehicle, the Coulomb-Micklethwaite equation can be modified as follows.

$$\tau = (c + p \tan \varphi)(\exp[(-k_2 + \sqrt{k_2^2 - 1})k_1j] - \exp[(-k_2 - \sqrt{k_2^2 - 1})k_1j]) \quad (3.5)$$

Where k_1 and k_2 are slip coefficients and j is the amount of soil deformation that produces stress τ .

The equation was approximated for soils that behave as a plastic by Janosi and Hanamoto [7] as follows.

$$\tau = (c + p \tan \varphi)(1 - e^{-j/k}) \quad (3.6)$$

Where k is the slip coefficient. c , φ and k are found from fitting curves into empirical data collected under simulated vehicle action.

Figure 3.2 represents the pressure under a tire.

3.2.2 Cone penetrometer

Another method of determining soil characteristics is the cone penetrometer as shown in Figure 3.3 , here the soil drag and soil thrust are lumped into one value called the cone index. cone index is defined in terms of the average load exerted by the soil upon a conical head forced into the ground to the depth to which the vehicle is expected to act. The head of the penetrometer is generally a 30-degree cone with a base area of 2

Mechanics of Pneumatic Tires

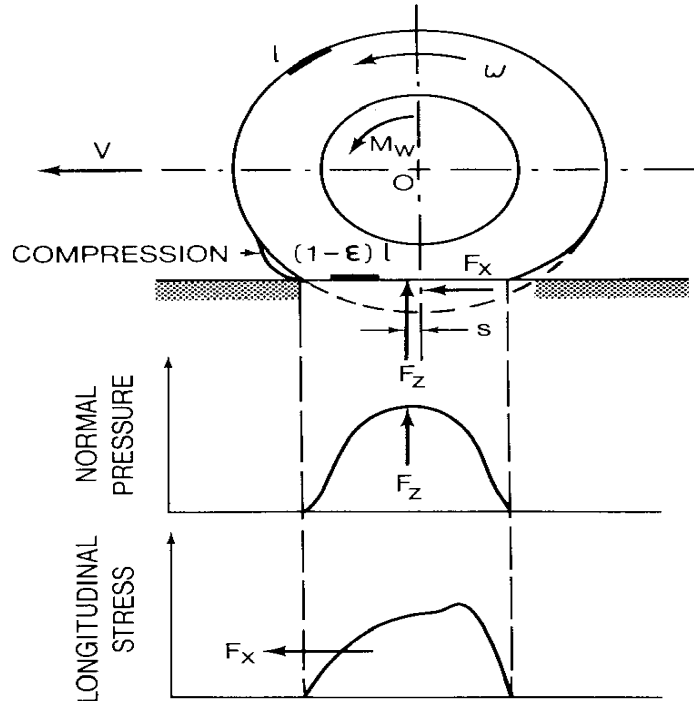


Figure 3.2: Pressure under the tire[7]

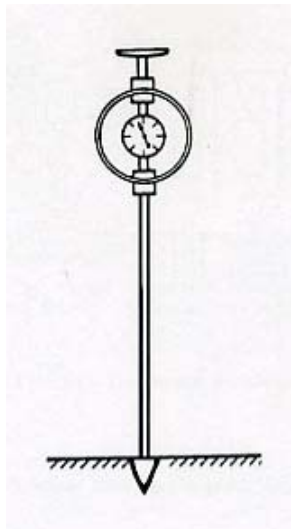


Figure 3.3: Cone penetrometer[9]

square inches. The cone index is empirically correlated with 'go,'no go' performance of many existing vehicles. The towing force is also empirically correlated with the cone index, at the moment immobilization appears maximum, towing force equals approximately the maximum soil thrust. The ratio of that force to vehicle weight also gives a measure of maximum negotiable slope[9].

The cone index does not discriminate between vehicle creep and high speed, it is commonly used by field operators who want to know whether their vehicle can move in a given area. The simplicity of the penetrometer make it possible to use it in studies of trafficability for remote and inaccessible areas.

Due to continuous loading and unloading, strength and soil characteristics sometimes change, due to this additional remolding test become necessary. In this a test a soil sample is remolded by drop hammering it, the cone index is measured before and after the remolding; the ratio between the original cone index(CI) to the remolded cone index is the remolding index(RI). Another concept of soil consistency is derived from this. The rating cone index expresses the soil strength at a point that is subjected to sustained traffic. It is given by the formulation,

$$RemoldedConeIndex = (ConeIndex * RemoldingIndex) \quad (3.7)$$

3.2.3 Penetrometer vs Bevameter

The differences between the penetrometer and bevameter methods are as follows

1. The bevameter technique applies to all soils and snows, it consist of a number of penetration and shear test, and measures a number of soil parameters. The penetrometer technique was conceived for measuring soil consistency in fine grained soil, measures only one parameter.
2. The correlation between the bevameter data and the vehicle design and performance parameters is achieved through experimentally tested mathematical model, whereas the correlation of cone indices with the 'go', 'no-go' parameters is achieved by empirical correlation.

3. Several parameters that are calculated using the bevameter method contain more information about the soil than the single parameter calculated using the cone penetrometer. Cone index does not provide enough information for concept or design evaluation of terrain vehicle systems.

The cone index(CI) can be calculated from the bevameters parameters k_c , k_φ , n . The approximate formulation is as follows

$$CI = 1.625 \left\{ \frac{k_c}{n+1} [(z+1.5)^{n+1} - z^{n+1}] + 0.517k_\varphi \left[\frac{(z+1.5)^{n+2}}{(n+1)(n+2)} + \frac{z^{n+2}}{n+2} - \frac{(z+1.5)z^{n+1}}{n+1} \right] \right\} \quad (3.8)$$

3.3 Model used in the research

The models used in this research follow Bekker's and Wong's formulae.

1. Homogenous soil :- In this type of soil it is assumed that the soil is homogenous by nature within the depth of interest. the sinkage pressure relationship is the one proposed by Bekker[9].

$$p_i = \left(\frac{k_c}{b} + k_\varphi \right) z^n \quad (3.9)$$

Where p , z represent the pressure and sinkage respectively, b is the smaller of the dimensions of the track. The rest are pressure sinkage parameters.

The shear due to this pressure is represented by

$$\tau^{sh} = c + p \tan(\phi^{sh}) (1 - e^{-\frac{c}{k^{sh}}}) \quad (3.10)$$

Where c is the cohesion of the soil, ϕ^{sh} is the soil angle of shearing.

2. Organic soil:- The organic terrain consist of a layer of living vegetables on the surface and a layer of peat below it. An empirical relationship for soil that fit this description was empirically calculated by Wong.

$$p_i = k_p z_i + \frac{4m_m z_i^2}{D_h} \quad (3.11)$$

Where z_i and p_i are the sinkage and pressure respectively, k_p is the stiffness parameter of the peat, m_m is a strength parameter for the surface layer, and D_h is called the hydraulic diameter of the contact area.

For organic soil, the shear stress initially increases with displacement and reaches a maximum where the "shear off" of the mat is initiated. The shear stress is given by

$$\tau^{sh} = \tau_{max}^{sh} \frac{j}{K_w} e^{1-(j/K_w)} \quad (3.12)$$

Where K_w is the shear displacement where the maximum shear stress τ_{max}^{sh} occurs.

Chapter 4

Vehicle model

4.1 Tracked vehicle model

Traditionally mathematical models created for tracked vehicles combined both the track and the vehicle to form one single model. This made it quiet difficult to change the track model to suit any other vehicle. Most models did not include large numbers of degrees of freedom for the sake of saving computing time. The complexity of the vehicle model depends on the amount of information one wants about the overall performance of the vehicle.

For the purpose of this study a recursive dynamics model [1] is chosen to simulate the vehicle. All computations are performed using relative coordinates. The model is simple and accurate for rigid body motion.

The track model is created as a separate module, such that it can be easily adapted to suit and any kind of of tracked vehicle combined with, the vehicle model,it helps us analyze whether the track model is able to correctly predict the track-terrain interaction for a tracked vehicle.

4.2 Formulation of the model

The trailer model developed in this study uses the recursive dynamics [1] for the formulation. This formulation is explained here for a pair of bodies with relative motion between them. Let $\mathbf{x}_0 \mathbf{y}_0 \mathbf{z}_0$ be the global coordinates for the system. Body i (inboard body) can be located by the position vector \mathbf{r}_i from the origin in the global frame to the origin (O_i) of the body frame $\mathbf{x}'_i \mathbf{y}'_i \mathbf{z}'_i$. \mathbf{A}_i is the transformation matrix, that transforms any vector in the body i reference frame to the global reference frame. A joint reference frame, $\mathbf{x}''_{ij} \mathbf{y}''_{ij} \mathbf{z}''_{ij}$, is defined and fixed on body i at the joint connection \mathbf{O}''_{ij} , which is located at a distance \mathbf{s}_{ij} from the origin \mathbf{O}_i . The origin (\mathbf{O}'_j) of joint reference frame $\mathbf{x}'_j \mathbf{y}'_j \mathbf{z}'_j$ of body j (outboard body) is located at a distance of \mathbf{d}_{ij} from the joint reference frame of body i . The joint reference frame of body j is also located, at a distance of \mathbf{r}_j from the origin of the system in the global reference frame.

Reference frames for each successive body in the kinematic chain are defined in the same way as those for body i .

The local coordinate reference frame of each body can be defined anywhere, generally it is more advantageous to place all the coordinate reference frames at the center of gravity.

The present vehicle model formulation considers the chassis to be the base body. All bodies except the chassis have both an inboard and an outboard body. The chassis is connected to the axle by a combination revolute-translational joint. The axle is connected to the left and right walking beams by means of revolute joints. The wheels are attached to the ends of the two walking beams using revolute joints. The configuration and the respective formulations will be explained later in the chapter. Except for the base body, all the reference frames are placed at the center of gravity.

4.2.1 Position analysis

Once position of body i is located, position of body j can be easily located by the position vector given by

$$\mathbf{r}_j = \mathbf{r}_i + \mathbf{s}_{ij} + \mathbf{d}_{ij} \quad (4.1)$$

In Eq(4.1) \mathbf{r}_i represents the global position of coordinate reference frame for body i , \mathbf{s}_{ij} represents the the body fixed vector from the body i reference frame to the joint reference frame of body i , \mathbf{d}_{ij} represents the vector that connects that connects the joint reference frame of body i to joint reference frame of body j . In Eq(4.1) all the vectors are expressed with respect to the global reference frame.

The vector \mathbf{s}'_{ij} is a fixed vector which connects the body reference frame to the joint reference frame of body i . It can be expressed as

$$\mathbf{s}_{ij} = \mathbf{A}_{ij}\mathbf{s}'_{ij} \quad (4.2)$$

where in the global reference frame \mathbf{A}_{ij} represents the transformation from body reference frame of i to the global reference frame, \mathbf{s}'_{ij} is a constant vector represented in the local coordinates. The vector \mathbf{d}_{ij} is represented as follows

$$\mathbf{d}_{ij} = \mathbf{A}_i\mathbf{C}_{ij}\mathbf{d}''_{ij} \quad (4.3)$$

In Eq (4.3) \mathbf{d}''_{ij} is the joint vector represented in terms of the joint reference frame of body i , \mathbf{C}_{ij} is the constant relative transformation matrix from body reference of body i to the joint reference frame. \mathbf{C}_{ij} is the orthonormal transformation matrix, in this study \mathbf{C}_{ij} is an identity matrix everywhere, except for the joint reference frames between the axle and the walking beams.

The global transformation matrix for body j can be represented as

$$\mathbf{A}_j = \mathbf{A}_i\mathbf{C}_{ij}\mathbf{A}_{ij} \quad (4.4)$$

where \mathbf{A}_{ij} represents the relative transformation between bodies i and j .

$$\mathbf{A}_{ij} = \begin{bmatrix} \cos \theta_j & -\sin \theta_j & 0 \\ \sin \theta_j & \cos \theta_j & 0 \\ 0 & 0 & 1 \end{bmatrix} \quad (4.5)$$

Where θ_j is the relative coordinate of the revolute joint.

4.2.2 Velocity analysis

The velocity of body j can be expressed using relative coordinates and velocities by differentiating Eq (4.1) with respect to time. It can be expressed as

$$\dot{\mathbf{r}}_j = \dot{\mathbf{r}}_i + \dot{\mathbf{s}}_{ij} + \dot{\mathbf{d}}_{ij} \quad (4.6)$$

by expanding $\dot{\mathbf{s}}_{ij}$ and $\dot{\mathbf{d}}_{ij}$ we can represent the same equation as follows

$$\dot{\mathbf{r}}_j = \dot{\mathbf{r}}_i + \dot{\mathbf{A}}_i \mathbf{s}'_{ij} + \dot{\mathbf{A}}_i \mathbf{C}_{ij} \mathbf{d}''_{ij} + \dot{\mathbf{A}}_i \mathbf{C}_{ij} \frac{\partial \mathbf{d}''_{ij}}{\partial \mathbf{q}_i} \dot{\mathbf{q}}_i \quad (4.7)$$

Where $\dot{\mathbf{q}}_i$ is the relative generalized coordinates of the joint connecting bodies i and j , $\dot{\mathbf{A}}_i$ is the time derivative of the body orientation matrix, which can be represented in terms of the local angular velocity, $\dot{\boldsymbol{\omega}}'_i$, or in terms of the global angular velocity, $\dot{\boldsymbol{\omega}}_i$, as follows

$$\dot{\mathbf{A}}_i = \mathbf{A}_i \dot{\boldsymbol{\omega}}'_i = \tilde{\boldsymbol{\omega}}_i \mathbf{A}_i \quad (4.8)$$

Where $\tilde{\boldsymbol{\omega}}$ is defined

$$\tilde{\boldsymbol{\omega}} = \begin{bmatrix} 0 & -\omega_z & \omega_y \\ \omega_z & 0 & \omega_x \\ \omega_y & \omega_x & 0 \end{bmatrix} \quad (4.9)$$

substituting this in Eq (4.7) we get the global velocity of body j in terms of the relative coordinates is

$$\dot{\mathbf{r}}_j = \dot{\mathbf{r}}_i + \tilde{\boldsymbol{\omega}}_i \mathbf{s}_{ij} + \tilde{\boldsymbol{\omega}}_i \mathbf{d}_{ij} + \frac{\partial \mathbf{d}_{ij}}{\partial \mathbf{q}_i} \dot{\mathbf{q}}_i \quad (4.10)$$

$$\dot{\mathbf{A}}_i \mathbf{C}_{ij} \frac{\partial \mathbf{d}''_{ij}}{\partial \mathbf{q}_i} = \frac{\partial \mathbf{d}_{ij}}{\partial \mathbf{q}_i} \dot{\mathbf{q}}_i \quad (4.11)$$

The body fixed joint reference frame vector \mathbf{s}_{ij} can be substituted in the velocity Eq (4.10) as $\mathbf{s}_{ij} = \mathbf{r}_j - \mathbf{r}_i - \mathbf{d}_{ij}$, thereby eliminating it. This is done as follows

$$\dot{\mathbf{r}}_j = \dot{\mathbf{r}}_i + \tilde{\boldsymbol{\omega}}_i(\mathbf{r}_j - \mathbf{r}_i - \mathbf{d}_{ij}) + \tilde{\boldsymbol{\omega}}_i \mathbf{d}_{ij} + \frac{\partial \mathbf{d}_{ij}}{\partial \mathbf{q}_i} \dot{\mathbf{q}}_i \quad (4.12)$$

$$\dot{\mathbf{r}}_j = \dot{\mathbf{r}}_i + \tilde{\boldsymbol{\omega}}_i \mathbf{r}_j - \tilde{\boldsymbol{\omega}}_i \mathbf{r}_i + \frac{\partial \mathbf{d}_{ij}}{\partial \mathbf{q}_i} \dot{\mathbf{q}}_i \quad (4.13)$$

$$\dot{\mathbf{r}}_j = \dot{\mathbf{r}}_i + \tilde{\mathbf{r}}_i \boldsymbol{\omega}_i - \tilde{\mathbf{r}}_j (\boldsymbol{\omega}_j - \boldsymbol{\omega}_{ij}) + \frac{\partial \mathbf{d}_{ij}}{\partial \mathbf{q}_i} \dot{\mathbf{q}}_i \quad (4.14)$$

Using the definition

$$\boldsymbol{\omega}_{ij} = \mathbf{H}_j(\mathbf{A}_i, \mathbf{q}_j) \dot{\mathbf{q}}_j \quad (4.15)$$

This can be substituted in the velocity equation to get are final form of the equation.

$$\dot{\mathbf{r}}_j + \tilde{\mathbf{r}}_{ij} \boldsymbol{\omega}_j = \dot{\mathbf{r}}_i + \tilde{\mathbf{r}}_i \boldsymbol{\omega}_i + \left(\frac{\partial \mathbf{d}_{ij}}{\partial \mathbf{q}_i} + \tilde{\mathbf{r}}_j \mathbf{H}_j(\mathbf{A}_i, \mathbf{q}_j) \right) \dot{\mathbf{q}}_j \quad (4.16)$$

$$\begin{bmatrix} \dot{\mathbf{r}}_j + \tilde{\mathbf{r}}_j \boldsymbol{\omega}_j \\ \boldsymbol{\omega}_j \end{bmatrix} = \begin{bmatrix} \dot{\mathbf{r}}_i + \tilde{\mathbf{r}}_i \boldsymbol{\omega}_i \\ \boldsymbol{\omega}_i \end{bmatrix} + \begin{bmatrix} \frac{\partial \mathbf{d}_{ij}}{\partial \mathbf{q}_i} + \tilde{\mathbf{r}}_j \mathbf{H}_j(\mathbf{A}_i, \mathbf{q}_j) \\ \mathbf{H}_j(\mathbf{A}_i, \mathbf{q}_j) \end{bmatrix} \dot{\mathbf{q}}_j \quad (4.17)$$

The equation can be written in a simpler format by substituting

$$\hat{\mathbf{Y}}_j = \begin{bmatrix} \dot{\mathbf{r}}_j + \tilde{\mathbf{r}}_j \boldsymbol{\omega}_j \\ \boldsymbol{\omega}_j \end{bmatrix} \quad (4.18)$$

and

$$\mathbf{B}_j = \begin{bmatrix} \frac{\partial \mathbf{d}_{ij}}{\partial \mathbf{q}_i} + \tilde{\mathbf{r}}_j \mathbf{H}_j(\mathbf{A}_i, \mathbf{q}_j) \\ \mathbf{H}_j(\mathbf{A}_i, \mathbf{q}_j) \end{bmatrix} \quad (4.19)$$

$\hat{\mathbf{Y}}_j$ is the state velocity vector and \mathbf{B}_j the velocity transformation matrix. Substituting this in Eq 4.17 we get

$$\hat{\mathbf{Y}}_j = \hat{\mathbf{Y}}_i + \mathbf{B}_j \dot{\mathbf{q}}_j \quad (4.20)$$

The Cartesian velocity vector, denoted \mathbf{Y}_k , can be expressed in terms of the state velocity vector, $\hat{\mathbf{Y}}_k$ as

$$\mathbf{Y}_k = \begin{pmatrix} \dot{\mathbf{r}}_k \\ \boldsymbol{\omega}_k \end{pmatrix} = \begin{bmatrix} I & -\tilde{\mathbf{r}}_k \\ 0 & I \end{bmatrix} \begin{pmatrix} \dot{\mathbf{r}}_k + \tilde{\mathbf{r}}_k \boldsymbol{\omega}_k \\ \boldsymbol{\omega}_k \end{pmatrix} \quad (4.21)$$

4.2.3 Acceleration analysis

The acceleration of the state velocity vector can be calculated by differentiating Eq (4.20) with respect to time.

$$\dot{\hat{\mathbf{Y}}}_j = \dot{\hat{\mathbf{Y}}}_j + \mathbf{B}_j \ddot{\mathbf{q}}_j + \dot{\mathbf{B}}_j \dot{\mathbf{q}}_j \quad (4.22)$$

The Cartesian acceleration vector can be derived from the state acceleration vector as follows,

$$\dot{\mathbf{Y}}_k = \begin{bmatrix} I & -\tilde{\mathbf{r}}_k \\ 0 & I \end{bmatrix} \dot{\hat{\mathbf{Y}}}_k + \begin{bmatrix} I & -\dot{\tilde{\mathbf{r}}}_k \\ 0 & I \end{bmatrix} \hat{\mathbf{Y}}_k \quad (4.23)$$

4.2.4 Joint formulation

The vehicle model that is presented in this study consist only of revolute and translation-revolute joints, therefore only the following joint formulations will be presented in this study.

Revolute joint

A revolute joint and the positions of its joint reference frames are presented in Figure 4.1. An assumption that is made in the derivation of the formulation of a revolute joint is that a pair of coordinates of the joint reference frames coincide.

Since \mathbf{d}_{ij} and \mathbf{d}_{ij}'' are equal to zero,

$$\mathbf{r}_j = \mathbf{r}_i + \mathbf{s}_{ij} \quad (4.24)$$

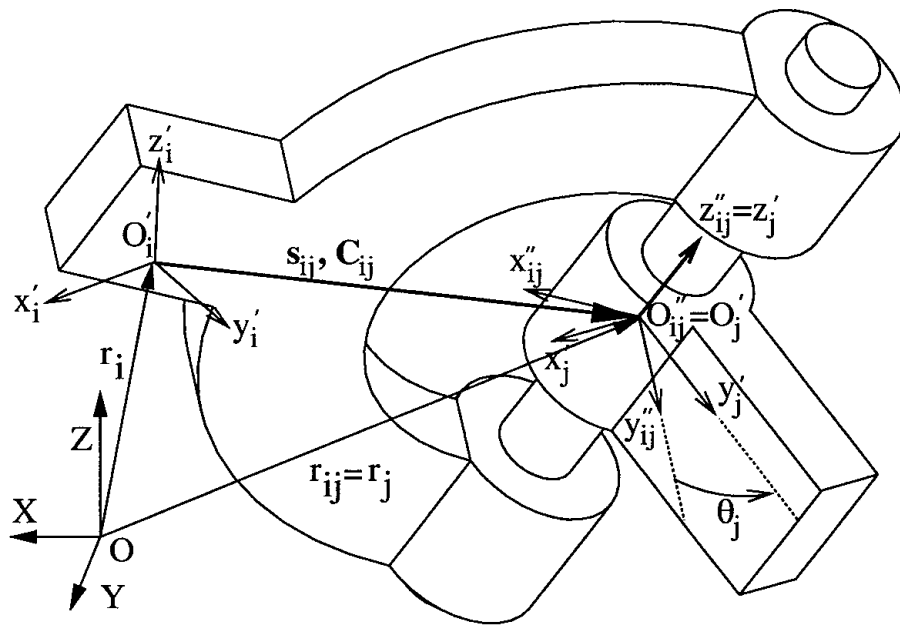


Figure 4.1: Revolute joint[1]

The transformation matrix \mathbf{A}_j for the joint is as following

$$\mathbf{A}_j = \mathbf{A}_i \mathbf{C}_{ij} \mathbf{A}_{ij} \quad (4.25)$$

Where \mathbf{A}_{ij} is an orthonormal rotation matrix about a single axis. The generalized coordinate associated with the joint is its rotation θ_j . In the figure, the axis of rotation is the Z axis

The rotation matrix for rotation about Z axis is given by

$$\mathbf{A}_{ij} = \begin{bmatrix} \cos(\theta_j) & -\sin(\theta_j) & 0 \\ \sin(\theta_j) & \cos(\theta_j) & 0 \\ 0 & 0 & 1 \end{bmatrix} \quad (4.26)$$

Revolute joint velocity analysis

Since the revolute joint as shown in Figure 4.1 is represented as a rotation about a single axis vector, the relative angular velocity between the bodies can be expressed as follows:

$$\boldsymbol{\omega}_{ij} = \mathbf{A}_{ij} \mathbf{C}_{ij} \boldsymbol{\omega}_{ij}'' = \mathbf{A}_{ij} \mathbf{C}_{ij} \mathbf{u}_{ij}'' \dot{\mathbf{q}}_j = \mathbf{u}_{ij} \dot{\mathbf{q}}_j \quad (4.27)$$

Where \mathbf{u}_{ij} is the unit vector about which the rotation occurs. In the figure this is the Z axis. By substituting this in Eq 4.15 we get the \mathbf{H}_j to be

$$\mathbf{H}_j(\mathbf{A}_i, \mathbf{q}_i) = \mathbf{u}_{ij} \quad (4.28)$$

Given that $\mathbf{d}_{ij} = 0$, \mathbf{B}_j the velocity transformation becomes

$$\mathbf{B}_j = \begin{bmatrix} \tilde{\mathbf{r}} \mathbf{u}_{ij} \\ \mathbf{u}_{ij} \end{bmatrix} \quad (4.29)$$

Revolute joint acceleration transformation

The remaining value that has to be calculated for a revolute joint is the $\dot{\mathbf{B}}_j \dot{\mathbf{q}}_j$, this term can be calculated by differentiating \mathbf{B}_j

$$\mathbf{D}_j = \begin{bmatrix} \dot{\tilde{\mathbf{r}}}_j \mathbf{u}_{ij} + \tilde{\mathbf{r}}_j \dot{\mathbf{u}}_{ij} \\ \dot{\mathbf{u}}_{ij} \end{bmatrix} \dot{\mathbf{q}}_j \quad (4.30)$$

substituting

$$\dot{\mathbf{u}}_{ij} = \tilde{\boldsymbol{\omega}}_i \mathbf{u}_{ij} \quad (4.31)$$

$$\mathbf{D}_j = \begin{bmatrix} \dot{\tilde{\mathbf{r}}}_j \mathbf{u}_{ij} + \tilde{\mathbf{r}}_j \tilde{\boldsymbol{\omega}}_i \mathbf{u}_{ij} \\ \tilde{\boldsymbol{\omega}}_i \mathbf{u}_{ij} \end{bmatrix} \dot{\mathbf{q}}_j \quad (4.32)$$

Translational joint

The assumption that is made in the translation joint is that one pair of axis are coincidental and oriented along the direction of translation as shown in Figure 4.2. The position of body j is calculated as follows

$$\mathbf{r}_j = \mathbf{r}_i + \mathbf{s}_{ij} + \mathbf{d}_j \quad (4.33)$$

The global transformation matrix for body j can be expressed as follows

$$\mathbf{A}_j = \mathbf{A}_i \mathbf{C}_{ij} \mathbf{A}_{ij} \quad (4.34)$$

For a translation joint the relative transformation, \mathbf{A}_{ij} is I.

By orienting \mathbf{d}_{ij} in the direction of translation we get

$$\mathbf{d}_{ij} = \mathbf{q}_j \mathbf{u}_{ij} \quad (4.35)$$

Where \mathbf{u}_{ij} is the direction of translation.

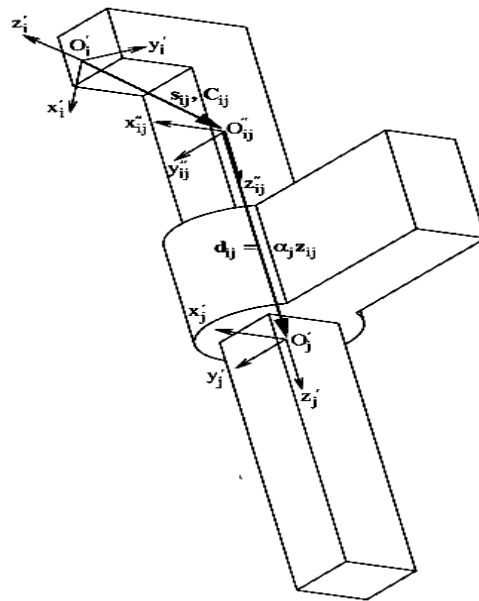


Figure 4.2: Translation joint[1]

Translational joint velocity transformation

Since the relative velocity of the two bodies connected by the translational joint is represented by a change in the length of the \mathbf{d}_{ij} vector; the relative angular velocity between the two bodies is zero, therefore \mathbf{A}_{ij}

$$\boldsymbol{\omega}_j = \boldsymbol{\omega}_i \quad (4.36)$$

$$\mathbf{H}_j(\mathbf{A}_i, \mathbf{q}_i) = 0 \quad (4.37)$$

The \mathbf{B}_j matrix can be expressed as

$$\mathbf{B}_j = \begin{bmatrix} \frac{\partial \mathbf{d}_{ij}}{\partial \mathbf{q}_i} \\ 0 \end{bmatrix} = \begin{bmatrix} \mathbf{u}_{ij} \\ 0 \end{bmatrix} \quad (4.38)$$

Translational joint acceleration transformation

The \mathbf{D}_j vector for a translational joint can be found by differentiating \mathbf{B}_j with respect to time as follows

$$\mathbf{D}_j = \begin{bmatrix} \dot{\mathbf{u}}_{ij} \\ 0 \end{bmatrix} \dot{\mathbf{q}}_j = \begin{bmatrix} \tilde{\boldsymbol{\omega}}_i \mathbf{u}_{ij} \\ 0 \end{bmatrix} \dot{\mathbf{q}}_j \quad (4.39)$$

4.3 Dynamic formulation of the vehicle model

The dynamic formulation of the vehicle model follows the principles presented in the NADS document [1].

The equation of motion for the tracked vehicle model can be written in a matrix format as follows,

$$\bar{\mathbf{M}}\ddot{\bar{\mathbf{q}}} = \bar{\mathbf{Q}} \quad (4.40)$$

Where $\bar{\mathbf{M}}$ is the articulated inertia matrix

$$\bar{\mathbf{M}} = \begin{bmatrix} \mathbf{K}_1 & \mathbf{K}_2\mathbf{B}_2 & \mathbf{K}_3\mathbf{B}_3 & \mathbf{K}_4\mathbf{B}_4 & \cdots & \mathbf{K}_8\mathbf{B}_8 \\ \mathbf{B}_2^T\mathbf{K}_2 & \mathbf{B}_2^T\mathbf{K}_2\mathbf{B}_2 & \mathbf{B}_2^T\mathbf{K}_3\mathbf{B}_3 & \cdots & \mathbf{B}_2^T\mathbf{K}_8\mathbf{B}_8 & \\ \mathbf{B}_3^T\mathbf{K}_3 & \mathbf{B}_3^T\mathbf{K}_3\mathbf{B}_2 & \mathbf{B}_3^T\mathbf{K}_3\mathbf{B}_3 & \mathbf{B}_3^T\mathbf{K}_4\mathbf{B}_4 & \cdots & 0 \\ \vdots & \vdots & \vdots & \vdots & \ddots & \vdots \\ \mathbf{B}_8^T\mathbf{K}_8 & \mathbf{B}_8^T\mathbf{K}_8\mathbf{B}_2 & 0 & 0 & \cdots & \mathbf{B}_8^T\mathbf{K}_8\mathbf{B}_8 \end{bmatrix} \quad (4.41)$$

$$\ddot{\mathbf{q}} = \begin{bmatrix} \ddot{\mathbf{x}} \\ \ddot{\mathbf{y}} \\ \ddot{\mathbf{z}} \\ \dot{\omega}_x \\ \dot{\omega}_y \\ \dot{\omega}_z \\ \ddot{\theta}_2 \\ \ddot{\theta}_3 \\ \vdots \\ \ddot{\theta}_8 \end{bmatrix} \quad (4.42)$$

$$\bar{\mathbf{Q}} = \begin{bmatrix} \mathbf{L}_1 \\ \mathbf{B}'_2(\mathbf{L}_2 - \mathbf{K}_2\mathbf{D}_2) \\ \mathbf{B}'_3(\mathbf{L}_3 - \mathbf{K}_3(\mathbf{D}_2 + \mathbf{D}_3)) \\ \mathbf{B}'_4(\mathbf{L}_4 - \mathbf{K}_4(\mathbf{D}_3 + \mathbf{D}_4)) \\ \mathbf{B}'_5(\mathbf{L}_5 - \mathbf{K}_5(\mathbf{D}_3 + \mathbf{D}_5)) \\ \mathbf{B}'_6(\mathbf{L}_6 - \mathbf{K}_6(\mathbf{D}_2 + \mathbf{D}_6)) \\ \mathbf{B}'_7(\mathbf{L}_7 - \mathbf{K}_7(\mathbf{D}_6 + \mathbf{D}_7)) \\ \mathbf{B}'_8(\mathbf{L}_8 - \mathbf{K}_8(\mathbf{D}_6 + \mathbf{D}_8)) \end{bmatrix} \quad (4.43)$$

The terms \mathbf{K}_i and \mathbf{L}_i are calculated from the equations given below,

$$\mathbf{K}_m = \sum_{i=m}^n \hat{\mathbf{M}}_i \quad (4.44)$$

$$\mathbf{L}_i = \mathbf{L}_{i+1} - \mathbf{K}_{i+1}\mathbf{D}_{i+1} + \hat{\mathbf{Q}}_i \quad (4.45)$$

For each body the mass matrix \mathbf{M}_i and the force vector \mathbf{Q}_i are given as the following

$$\mathbf{M}_i = \begin{bmatrix} m_i I & -m_i \bar{\rho}_i \\ m_i \bar{\rho}_i & J_i \end{bmatrix} \quad (4.46)$$

$$\mathbf{Q}_i = \begin{bmatrix} F_i - m_i \tilde{\omega}_i \tilde{\omega}_i \rho_i \\ \eta_i - \tilde{\omega}_i J_i \omega_i \end{bmatrix} \quad (4.47)$$

For each body the generalized velocity state mass matrix, $\hat{\mathbf{M}}_i$, and the generalized force vector, $\hat{\mathbf{Q}}_i$ are expressed in terms of \mathbf{M}_i , \mathbf{Q}_i and the state transformation matrix \mathbf{T}_i as stated below

$$\hat{\mathbf{M}}_i = \mathbf{T}_i' \mathbf{M}_i \mathbf{T}_i = \begin{bmatrix} m_i I & -m_i(\tilde{r}_i + \tilde{\rho}_i) \\ m_i(\tilde{r}_i + \tilde{\rho}_i) & J_i - m_i(\tilde{r}_i \tilde{r}_i + \tilde{\rho}_i \tilde{r}_i + \tilde{r}_i \tilde{\rho}_i) \end{bmatrix} \quad (4.48)$$

$$\hat{\mathbf{Q}}_i = \mathbf{T}_i'(\mathbf{Q}_i + \mathbf{M}_i \mathbf{R}_i) = \begin{bmatrix} F_i + m_i \tilde{r}_i \omega_i - m_i \tilde{\omega}_i \tilde{\omega}_i \rho_i \\ \eta_i + \tilde{r}_i F_i - \tilde{\omega}_i J_i \omega_i + m_i \tilde{\rho}_i \dot{\tilde{r}}_i \omega_i + m_i \tilde{r}_i \dot{\tilde{r}}_i \omega_i - m_i \tilde{r}_i \tilde{\omega}_i \dot{\tilde{\omega}}_i \rho_i \end{bmatrix} \quad (4.49)$$

Where \mathbf{m}_i is the mass of body, ρ_i is the distance from the joint to the center of gravity, \mathbf{J}_i is the inertia of the body in the global reference frame, \mathbf{F}_i is the total force applied to body i and η_i is the total torque applied to the body i .

4.4 External forces

4.4.1 Translational spring damper actuators

The leaf springs in this trailer are modeled as a translational spring damper actuators, these are placed in-between the base body and the axle. The forces acting between the pair of bodies are equal and opposite. The co-ordinates for TSDA are shown in Figure 4.3. \mathbf{P}_i and \mathbf{P}_j are locations where the ends of the TSDA are connected. The vector \mathbf{d}_{ij} is the distance between them and is calculated as follows,

$$\mathbf{d}_{ij} = \mathbf{r}_j + \mathbf{s}_{ji} - \mathbf{r}_i - \mathbf{s}_{ij} \quad (4.50)$$

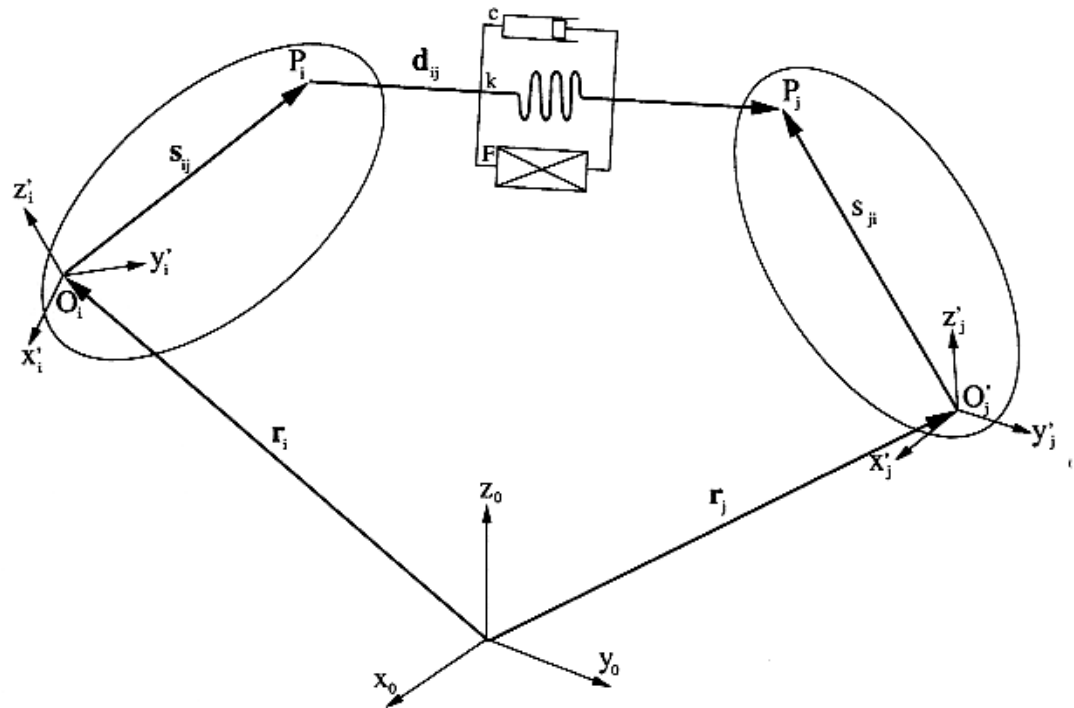


Figure 4.3: Translation spring damper actuators[1]

The length between the two point is given by,

$$l = (d_{ij}^T d_{ij})^{\frac{1}{2}} \quad (4.51)$$

The rate of change of length is as follows,

$$\dot{l} = \frac{1}{L} d_{ij}^T (\dot{\mathbf{r}}_j - \tilde{\mathbf{s}}_{ji} \boldsymbol{\omega}_j - \dot{\mathbf{r}}_i + \tilde{\mathbf{s}}_{ij}) \quad (4.52)$$

The magnitude of the force is,

$$f = k(l - l_0) + c\dot{l} \quad (4.53)$$

where c is the damping coefficient and k is the spring constant. The corresponding Cartesian space generalized forces acting on body i and j are

$$\mathbf{Q}_i = \frac{f}{l} \begin{bmatrix} \mathbf{d}_{ij} \\ \tilde{\mathbf{s}}_{ij} \mathbf{d}_{ij} \end{bmatrix} \quad (4.54)$$

$$\mathbf{Q}_j = -\frac{f}{l} \begin{bmatrix} \mathbf{d}_{ij} \\ \tilde{\mathbf{s}}_{ij} \mathbf{d}_{ij} \end{bmatrix} \quad (4.55)$$

4.4.2 Rotational spring damper actuator

The rotational spring damper actuators (RSDA) is shown in Figure (4.4). The friction between the axle and the walking beam is modeled using an RSDA. The RSDA generates a torque between the pair of bodies. The magnitude of torque

$$n = k_\theta(\theta - \theta_0) + c_\theta \dot{\theta} \quad (4.56)$$

Where k_θ is the spring constant, c_θ is the damping coefficient. Due to the fact that this is used to model friction damping, the stiffness factor is made zero $k_\theta = 0$. The torque vector acts along \mathbf{u}_{ij} , the axis of rotation of the joint connecting bodies i and j .

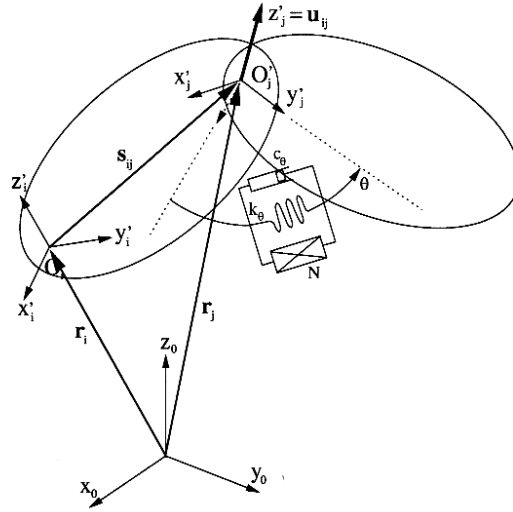


Figure 4.4: Rotational spring damper actuator[1]

The velocity state space generalized forces associated with the RSDA are

$$\hat{Q}_i = \begin{bmatrix} 0 \\ nu_{ij} \end{bmatrix} \quad (4.57)$$

$$\hat{Q}_j = - \begin{bmatrix} 0 \\ nu_{ij} \end{bmatrix} \quad (4.58)$$

4.5 The layout and algorithm for the current model

The layout of the trailer is shown as a tree-structure in Figure 4.5 starting from the base body, the layout shows,

1. Frame
2. Translation revolute joint that connects the Frame to the axle
3. Axle
4. Revolute joints that connect the axle to the walking beams

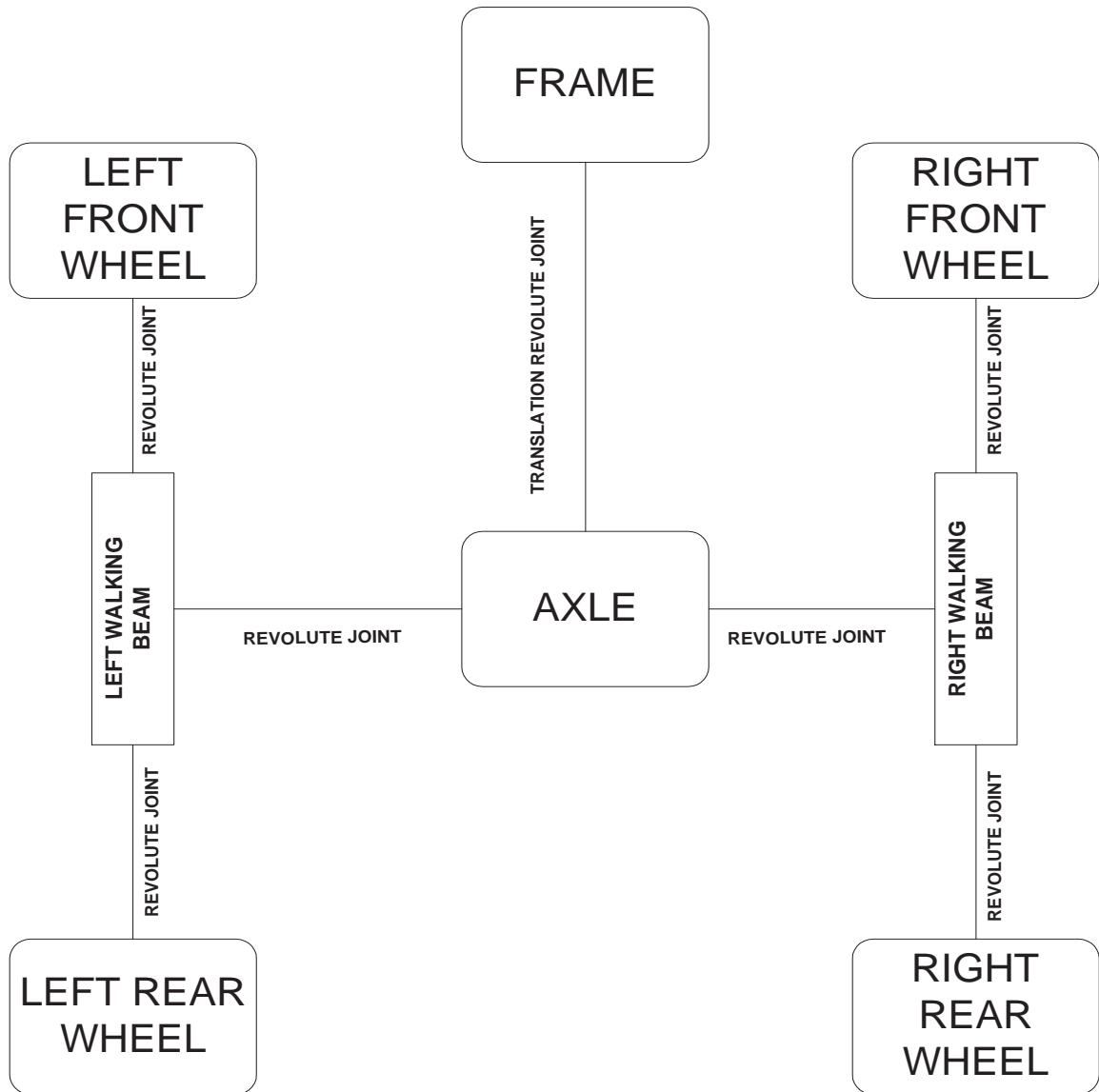


Figure 4.5: Layout of the vehicle

5. Walking beams
6. Revolute joints connecting the walking beam to the wheels
7. Wheels

Chapter 5

Track model

This chapter details the rubber band track model used. It is a dynamic, spatial model, the model takes into account the moment of inertia of the road wheels, shear between the track and the road. The suspension components of the vehicle are also taken into account and is modeled using a translation spring damper actuators. It takes into account the tire deformation and develops a complete track connectivity algorithm.

5.1 Model description

There are many types of tracks available like Continuous rubber belts, Metal tracks, Track with grouser. There are many environments where tracked vehicles are used and there are also different design criteria. This model is designed to represent continuous elastic track belts .

The rubber band track model has one degree of freedom, the model is used for straight line testing with without obstacles, rough terrain and different soil characteristics, the model does not give results for steering maneuvers. The shear force is calculated by taking the track terrain interaction with the soil, this depends on the soil characteristics the sinkage of the vehicle. The model does not take into account the vibration modes of the track.

The track model is completely described by:

1. Track-wheel-terrain interaction – This defines the forces on the track due to the track terrain interaction, forces on the wheel due to the interaction between the

wheel and the terrain; and the interaction between the track and the wheel.

2. Track connectivity algorithm – This defines how the track wraps around the wheels and terrain features, takes into account the various possible track terrain situations.
3. Soil model – This describes the terrain type and its features, this is essential to model the track-terrain interaction accurately

The principle difference between this model and the previously described ones is that this model involves deformable tires. The deformable tire in this model is modeled using a radial spring tire model. The track is modeled as discrete elements such that their interaction with the ground as well as the interaction of the track with the radial springs of the tire. There are few assumptions made with the track terrain interaction, it is assumed that the soil is plastic by nature and there is no rebound, this is done due to the fact that there is no terrain model that accurately models the rebound in terrain; this assumption does not affect the model due to the fact that most soils tend to act like a plastic material rather than elastic model; the other assumption is that the bumps in the terrain are made of concrete, this assumption is made due to the nature of the test course. The terrain data also has no memory of previous deformations.

The algorithm that is followed in this model is as follows.

1. Locate the positions of the two wheels and calculate the positions of the radial springs of the tire
2. Calculate the tire deflection and the tire forces generated due to it
3. Locate the positions of each of the track elements
4. Calculate the shear forces generated due to track terrain interaction
5. Calculate the tension in each track element
6. Calculate the forces due to the track tension

7. Calculate the change in length in the track, using which calculate the track tension for the next time step

5.2 Location of the radial springs, calculation of tire deflections and tire forces

The location of the tire and the joint location of the walking beams are found from the multi-body vehicle model at each time step. Using the following locations and the rotation of the walking beam the positions of the radial springs relative to the wheel center are calculated as follows

$$x_i = \sin(i * 5) * (R + t) \quad (5.1)$$

$$y_i = 0 \quad (5.2)$$

$$z_i = \cos(i * 5) * (R + t) \quad (5.3)$$

Where R is the radius of the tire and t is the thickness of the track, x_i , y_i and z_i are the relative positions of the radial spring element. The entire tire is described by radial springs set 5 degrees apart.

$$\mathbf{d}_i = [x_i, y_i, z_i] \quad (5.4)$$

$$\mathbf{D}_i = \mathbf{r}_w + \mathbf{A}d_i \quad (5.5)$$

Where \mathbf{D}_i is the global position of the radial spring element \mathbf{r}_w is the position of the wheel and \mathbf{A} is the rotation about the walking beam Here \mathbf{A} is a rotation about the y axis, given as

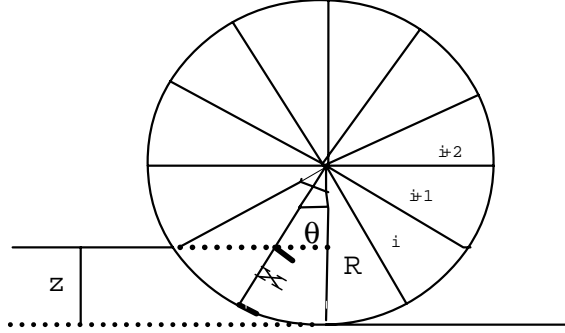


Figure 5.1: Tire deflection

$$A = \begin{bmatrix} \cos \theta & -\sin \theta & 0 \\ \sin \theta & \cos \theta & 0 \\ 0 & 0 & 1 \end{bmatrix} \quad (5.6)$$

As per Figure (5.1) we can calculate the tire deflection

$$\cos \theta_i = \frac{R - Z}{R - X} \quad (5.7)$$

$$R - Z = R \cos \theta_i - X \cos \theta_i \quad (5.8)$$

$$X = (R \cos \theta - R + Z) / \cos \theta_i \quad (5.9)$$

Since the soil is plastic by nature the ground level for the second tire will be different from the ground level for the first tire, this is taken into account by adding the ground level to the formulation. This is illustrated in Figure(5.2)

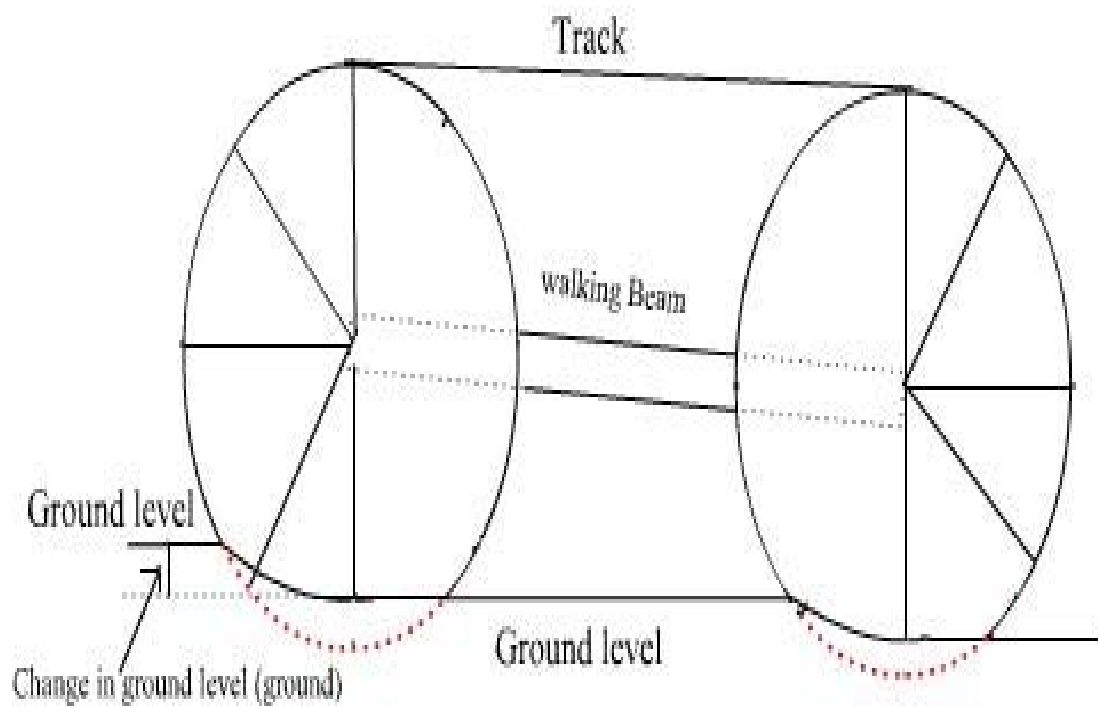


Figure 5.2: Ground profile

$$X = \frac{(R \cos \theta_i - R + Z + \text{ground})}{\cos \theta_i} \quad (5.10)$$

Taking the vertical displacement Z_i into account the formula changes as follows.

$$X = \frac{(R \cos \theta_i - R + Z + \text{ground} - Z_i)}{\cos \theta_i} \quad (5.11)$$

For each time step the undeflected positions of the radial springs are calculated. The deflected length of the radial springs are calculated by equating the forces generated by the radial springs and the force generated by the soil due to sinkage. Due to the fact that the pressure generated by the soil sinkage is a nonlinear equation it cannot be solved using matrices, so a simple iterative method is used to equate the forces generated by sinkage and forces due to tire deflections.

$$ts * def_i = ss * sinkage_i^n \quad (5.12)$$

Where def and $sinkage$ are the tire deflection and the soil sinkage respectively, ts is the stiffness of the radial spring and ss is the soil stiffness.

$$ss = (K_c/b + K_\phi) \quad (5.13)$$

K_c and K_ϕ are soil constants, b is the width of the tire.

The horizontal and vertical forces generated are as follows

$$F_h = \sum_{i=1}^n ts * X_i * \sin \theta_i \quad (5.14)$$

$$F_v = \sum_{i=1}^n ts * X_i * \cos \theta_i \quad (5.15)$$

F_v and F_h are the vertical and horizontal forces generated by the tire deflection.

5.3 Track connectivity algorithm

After the deflection of the tires are calculated, the position of the track can be found. The track is divided into many massless units. The track is made of three components; The component around the first tire, the component track between the wheels, the component around the second tire. To make the solution for the component around the tires easier, each track unit is associated with a radial spring.

Track around the front tire

The vertical and horizontal positions of the track around the tire is found using Eq 5.5 are as follows

$$t_x = D_{ix} \quad (5.16)$$

$$t_y = D_{iy} \quad (5.17)$$

$$t_z = D_{iz} - def_i \quad (5.18)$$

$$\mathbf{t}_i = [t_x, t_y, t_z] \quad (5.19)$$

Track between the wheels

The track between the wheels is divided into a fixed number of units. The location of these units are calculated from the last unit in contact with the tire. The direction of the tangent to the last element \mathbf{C} is used, the assumption is that the track is tangential to the tire. The distance

The following algorithm is used to calculate the position of the track elements

$$\mathbf{t}_{i+n} = \mathbf{t}_n + C * nu * j$$

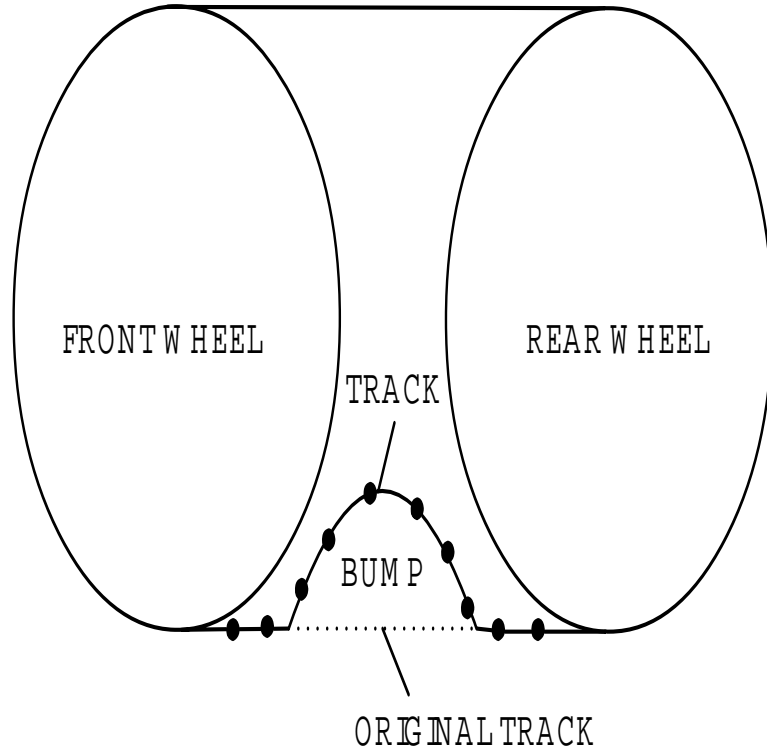


Figure 5.3: Bump between the wheels

where C is the tangential direction and nu is distance between the wheels divided number of track elements between the wheels.

If the height of the track element is less than the ground level plus the height of the terrain the it is assumed that the track element is on the surface, otherwise the track element follows the ground profile as shown in Figure 5.3

IF $t_{(i+n)z} < ground + Z$ then $t_{(i+n)z} = ground + Z$ ELSE it remains the same

If the horizontal position of the track element lies within the horizontal extremes of the front tire then it is checked whether the vertical position of the track element falls inside the tire, if so it is changed to fit the tire profile as shown in fig 5.4.

$$IF t_{(i+n)z} > \sqrt{R_f^2 + t_{(i+n)x}^2} \text{ then } t_{(i+n)z} = \sqrt{R_f^2 + t_{(i+n)x}^2}$$

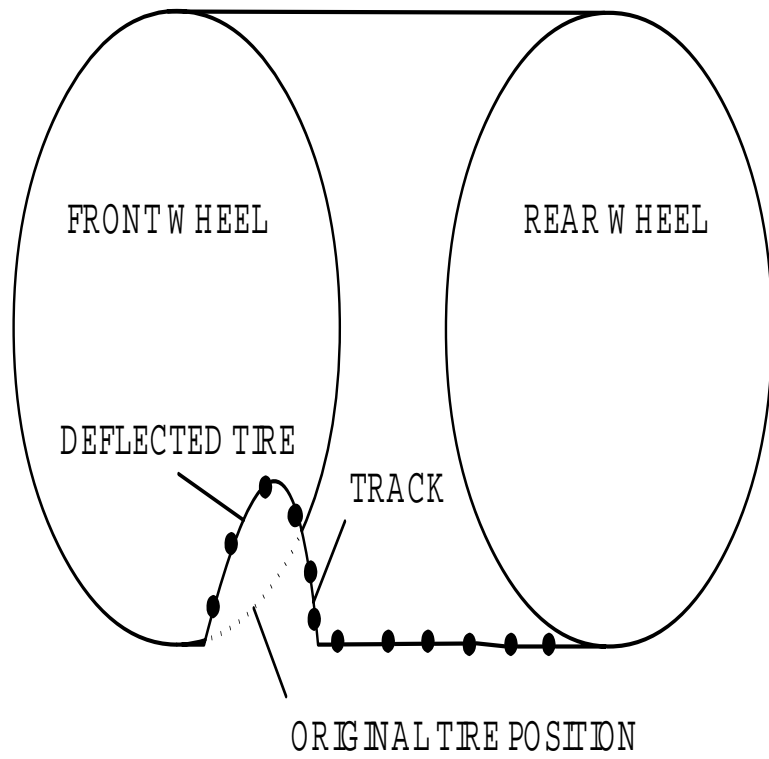


Figure 5.4: Tire on top of bump

If the horizontal position of the track element lies within horizontal extremes of the rear tire, then it is checked whether the vertical position of the track element falls inside the tire, if so it is changed to fit the undeflected tire position and this is the position of the undeflected position of the radial spring. The position of the track is calculated after calculating the deflection of the radial spring.

$$IF t_{(i+n)z} > \sqrt{R_f^2 + t_{(i+n)x}^2} \text{ then } t_{(i+n)z} = \sqrt{R_f^2 + t_{(i+n)x}^2}$$

where $t_{(i+n)z}$ is the undeflected length, after the tire deflection is calculated

$$t_{(i+n)z} = t_{(i+n)z} - def_{i+n}$$

Track around the second tire

The track around the second tire is wrapped the same way as the track around the first tire, where each element is associated with a radial spring.

$$t_x = D_{ix} \tag{5.20}$$

$$t_y = D_{iy} \tag{5.21}$$

$$t_z = D_{iz} - def_i \tag{5.22}$$

$$\mathbf{t}_{(n+nu)+i} = [t_x, t_y, t_z] \tag{5.23}$$

5.4 Forces generated by track terrain interaction

In this model it is assumed that there is no slip between the tire and the track, therefore the forces generated by the track is essentially is done by the shear forces generated by the interaction of the track with the terrain.

The slip of the track is calculated by using the following formulation.

$$AVt_i = Vbb + \tilde{\omega}_{wb}post_i \quad (5.24)$$

$$TV = r_i * \omega_{wheel} \quad (5.25)$$

Since this model is not designed to simulate turns, we only calculate the horizontal slip.

$$slip = 1 - AVt_i/TV \quad (5.26)$$

Where AVt_i is the actual track velocity for track element i , Vbb is the velocity of the base body, ω is the rotational velocity of the walking beam and $post_i$ is the distance from the walking beam to the track element, TV is the theoretical track velocity. Using the track slip and the pressure under the track we can calculate the shear force for homogenous soil using the Janosi-Hanamoto [9] approximation. The shear stress produced is as follows.

$$\tau^{sh} = \tau_{max}^{sh} (1 - e^{-\frac{slip}{k^{sh}}}) \quad (5.27)$$

$$\tau^{sh} = (c + p \tan(\phi^{sh})) (1 - e^{-\frac{slip}{k^{sh}}}) \quad (5.28)$$

Where p is the pressure under the track, c is the constant which depends on the water content.

The shear stress of the track between the wheels is calculated by calculating the normal force on the ground due to the bending of the track around the bump.

$$shear = K * Slip \quad (5.29)$$

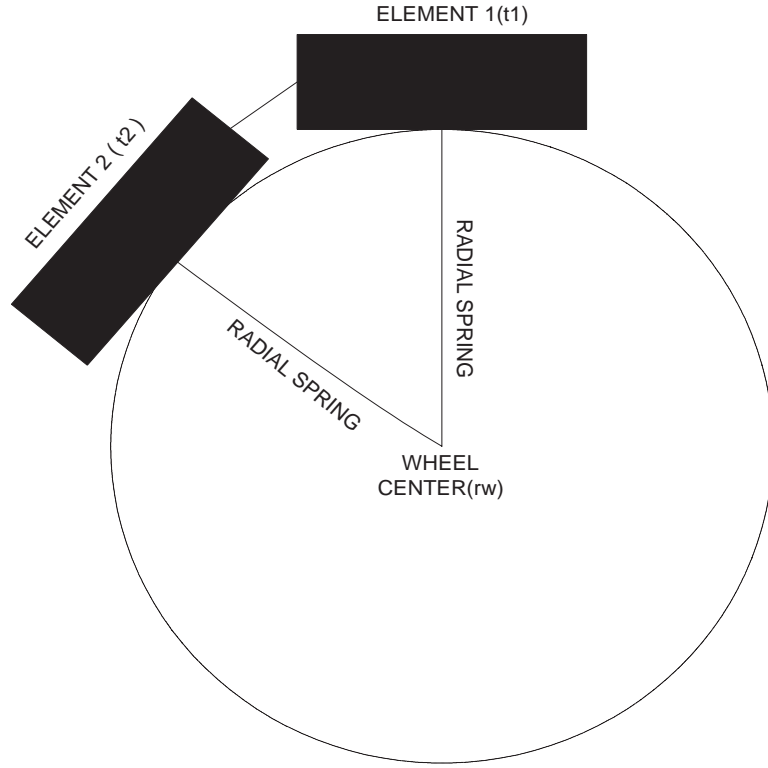


Figure 5.5: Track elements

5.5 Track tension

As per the free body diagram of each track element around the tire as shown in Figure (5.5). For each equation the forces are balanced, For the first element

$$T_1 * \begin{bmatrix} t_{1x} - t_{2x} \\ t_{1z} - t_{2z} \end{bmatrix} + F * \begin{bmatrix} t_{1x} - rw_x \\ t_{1z} - rw_z \end{bmatrix} = T_o * \begin{bmatrix} C_1 \\ C_3 \end{bmatrix} \quad (5.30)$$

For the other elements the formulation is as below

$$T_i * \begin{bmatrix} t_{ix} - t_{(i-1)x} \\ t_{iz} - t_{(i-1)z} \end{bmatrix} + F * \begin{bmatrix} t_{ix} - rw_x \\ t_{iz} - rw_z \end{bmatrix} + T_{(i+1)} * \begin{bmatrix} t_{ix} - t_{(i+1)x} \\ t_{iz} - t_{(i+1)z} \end{bmatrix} \quad (5.31)$$

$$= \begin{bmatrix} \tau_{sh} \\ 0 \end{bmatrix} \quad (5.32)$$

For the elements between the wheels,

$$T_i * \begin{bmatrix} t_{ix} - t_{(i-1)x} \\ t_{iz} - t_{(i-1)z} \end{bmatrix} + F * \begin{bmatrix} 0 \\ 1 \end{bmatrix} + T_{(i+1)} * \begin{bmatrix} t_{ix} - t_{(i+1)x} \\ t_{iz} - t_{(i+1)z} \end{bmatrix} \quad (5.33)$$

$$= \begin{bmatrix} \tau_{sh} \\ 0 \end{bmatrix} \quad (5.34)$$

The whole tension matrix, The following substitutions in notation $K_{rix} = t_{1x} - rw_x$, $K_{iz} = t_{1z} - rw_z$, $K_{tix} = t_{ix} - t_{(i+1)x}$, $K_{tiz} = t_{iz} - t_{(i+1)z}$

$$\mathbf{T} = \begin{bmatrix} K_{r1x} & K_{t1x} & 0 & 0 & \cdots & \cdots & 0 & 0 & 0 & 0 \\ K_{r1z} & K_{t1z} & 0 & 0 & \cdots & \cdots & 0 & 0 & 0 & 0 \\ 0 & -K_{t1x} & K_{r1x} & K_{t2x} & \cdots & \cdots & 0 & 0 & 0 & 0 \\ 0 & -K_{t1x} & K_{r1x} & K_{t2x} & \cdots & \cdots & 0 & 0 & 0 & 0 \\ \vdots & \vdots & \vdots & \ddots & \ddots & \ddots & \ddots & \ddots & \vdots & \vdots \\ 0 & 0 & 0 & \cdots & \cdots & -K_{t(i-1)x} & 0 & K_{tix} & 0 & \cdots \\ 0 & 0 & 0 & 0 & 0 & -K_{t(i-1)z} & 0 & K_{tiz} & 0 & \cdots \\ \vdots & \vdots & \vdots & \ddots & \ddots & \ddots & \ddots & \ddots & \ddots & \vdots \\ 0 & 0 & 0 & 0 & \cdots & \cdots & \cdots & -K_{t(i-1)z} & K_{r1z} & K_{tiz} \end{bmatrix} \quad (5.35)$$

$$\mathbf{U} = \begin{bmatrix} F_1 \\ T_1 \\ \vdots \\ \vdots \\ F_n \\ T_n \end{bmatrix} \quad (5.36)$$

$$\mathbf{B} = \begin{bmatrix} C_x * To \\ C_z * To \\ \tau_i \\ 0 \\ \vdots \\ \tau_n \\ 0 \end{bmatrix} \quad (5.37)$$

$$TU = B \quad (5.38)$$

The track tension for the next time step is the initial track tension plus the tension change due to the change in length.

$$To = To + (originallength - currentlength) * K2 \quad (5.39)$$

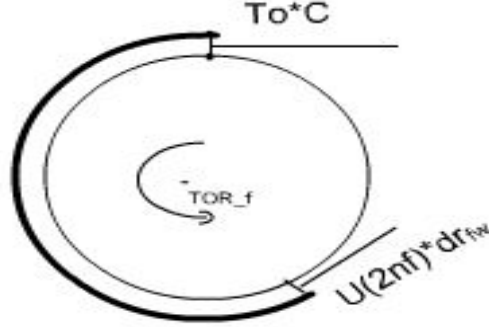


Figure 5.6: Torque around the wheels

Forces due to the tension on the vehicle

The values of U give the force along the direction of the track and along the direction of the radial spring or the normal to the ground. These forces are used to calculate the torque for each wheel, horizontal and vertical forces due to the track tension.

For calculating the torque about the front tyre, we have to locate the last element in contact with the tire d_{nf} , since in this model the tension is always considered to act along the track, we locate the direction between last element in contact with the tire and next element (dr_{fw}). The track is assumed to be always tangential to the tyre on the top. Therefore knowing both the directions and forces we can calculate the torque. for the front tire as shown in Figure (5.6).

Torque at the wheels is

$$Tor_f = \tilde{d}_{nf}(dr_{fw} * U(2nf)) - \tilde{d}_1(C * To) \quad (5.40)$$

Similarly the torque for the rear tire is

$$Tor_r = \tilde{d}_{nr}(dr_{rw} * U(2nr)) - \tilde{d}_n(C * U(2n)) \quad (5.41)$$

The tension also produces a horizontal force which will try and slow the vehicle, this

force also manifest itself as the drawbar pull on the vehicle and a vertical force.

Since we know the forces due to tension in the direction of radial springs their components in the horizontal and vertical direction can be easily calculated. Forces due to tension on the tires,

$$\begin{bmatrix} horizontal_i \\ vertical_i \end{bmatrix} = \begin{bmatrix} U(2i - 1) * t_{ix} - rw_x \\ U(2i - 1) * t_{iz} - rw_z \end{bmatrix} \quad (5.42)$$

The total horizontal and vertical forces are

$$horizontal = \sum_{i=1}^n horizontal_i \quad (5.43)$$

$$vertical = \sum_{i=1}^n vertical_i \quad (5.44)$$

5.6 The algorithm

1. The locations of all wheels are obtained from the vehicle model
2. The locations of all the radial springs are calculated for the tires
3. The tire deflection of the front tire is calculated
4. The location of the track elements around the front tire and the between the wheels are calculated
5. The new ground level is calculated
6. The tire deflection of the rear tire is calculated
7. The position of the track elements around the rear tire are calculated
8. The slip and shear for all track elements are calculated
9. The tension matrix is formed and the new tensions are calculated

10. Torque, horizontal and vertical forces are calculated for both the wheels
11. New track length is calculated to determine the tension for the next time step

Chapter 6

Results

The trailer is expected to perform in desert conditions, therefore the model is tested in sand and sandy loam at various speeds. Since there is no test data available there is no way the simulation results can be validated, therefore the simulation data are qualitatively compared to what might be expected for a vehicle running on the ground. The shear stress generated and the sinkage of the vehicle is compared with the theoretical values and available data for comparative vehicles.

6.1 Test of trailer model without the track model

First the vehicle model is tested to see whether it is able to run on the ground. The following test are run on the trailer vehicle model, with the tire represented as a single spring. The track model is not included in this set of simulations To test the initial vehicle model dynamic settling is done. The trailer is then dragged at slow and high speeds. No particular soil type is used to test the trailer model. The ground is assumed to infinitely stiff and thereby only the tires deflect. The height of ground is 0.

The simulation is run as follows

1. The vehicle model is dropped from a certain height.

The Figure (6.1) represents the position of the center of gravity on the Z, Figure (6.2) and Figure (6.3) represent the position of center of gravity of the axle on the Z and the length of the translation joint.

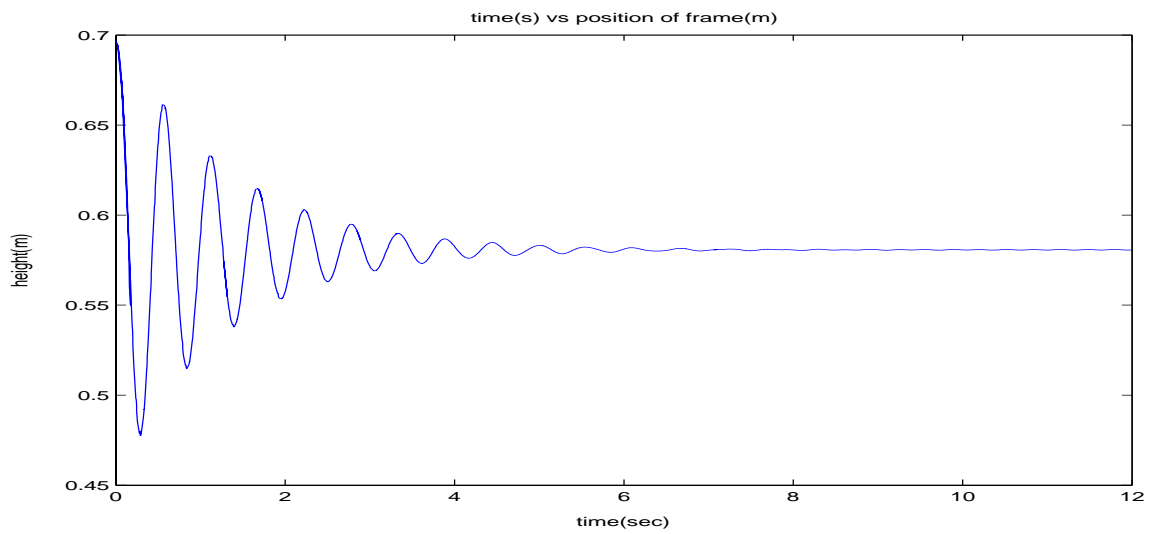


Figure 6.1: Vertical position of frame(dropped)

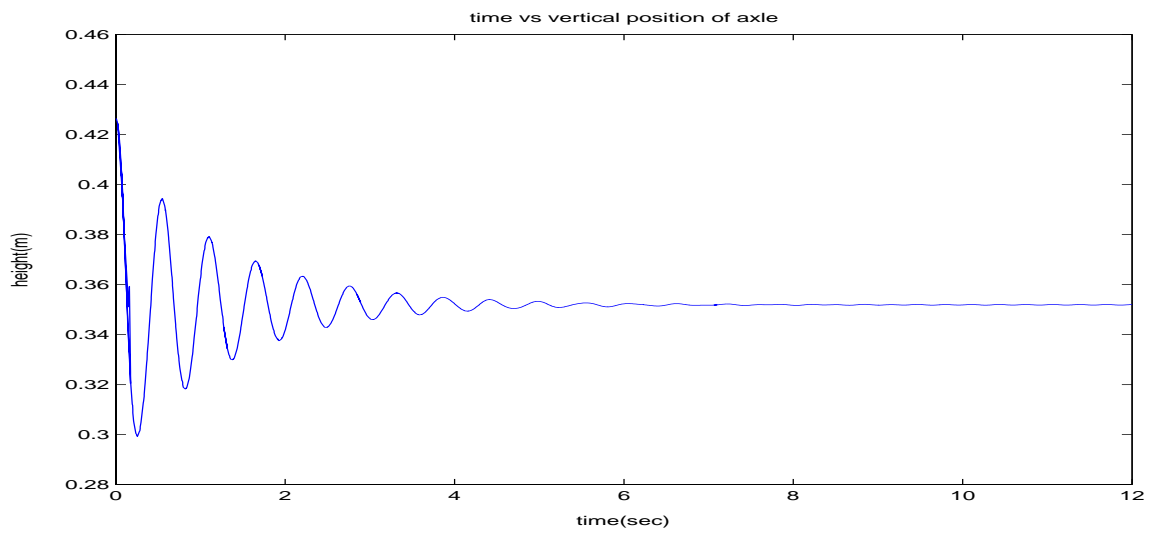


Figure 6.2: Vertical position of axle(dropped)

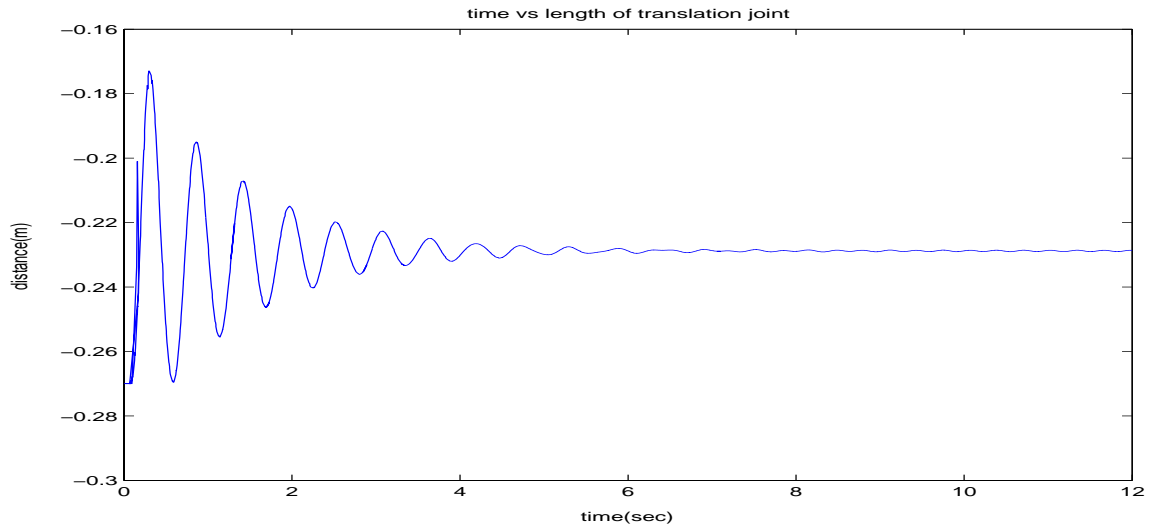


Figure 6.3: Length of translation joint(dropped)

- The trailer model is dragged at slow and high speed ([1 m/s-3.6 km/h] and [10 m/s-36 km/h])

Figures 6.4 and Figure 6.5 represent the center of gravity of the frame on the Z and the horizontal position of the center of gravity of the frame respectively when the trailer is run on flat terrain at a velocity of 1 m/s without the track elements. The ground level is zero.

Figures 6.6 and Figure 6.7 represent the center of gravity of the frame on the Z and the horizontal position of the center of gravity of the frame respectively when the trailer is run on flat terrain at 10 m/s without the track elements. The ground level is zero.

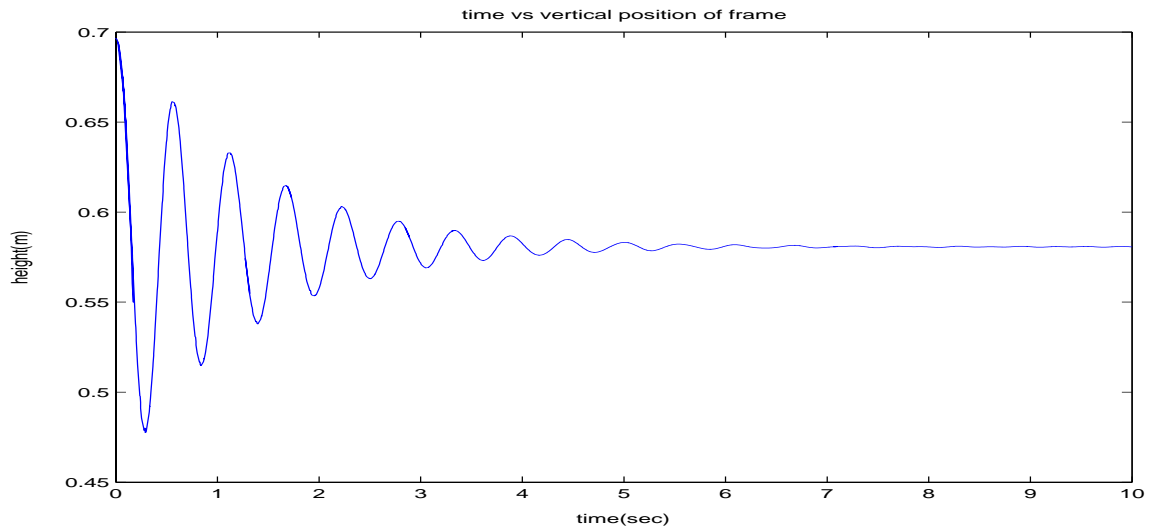


Figure 6.4: Vertical position of frame(1m/s)

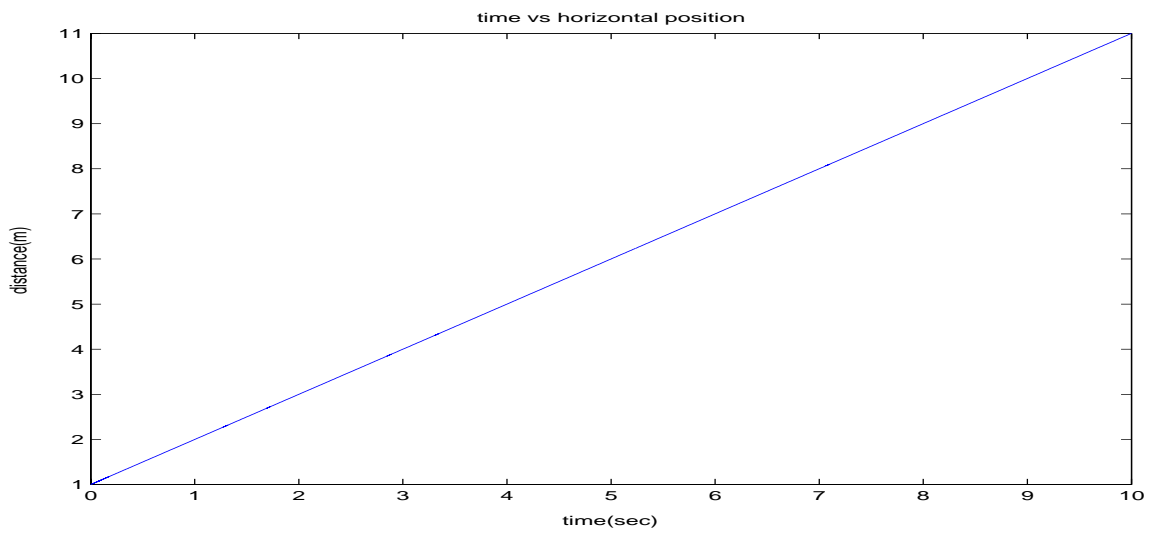


Figure 6.5: Horizontal position of axle(1m/s)

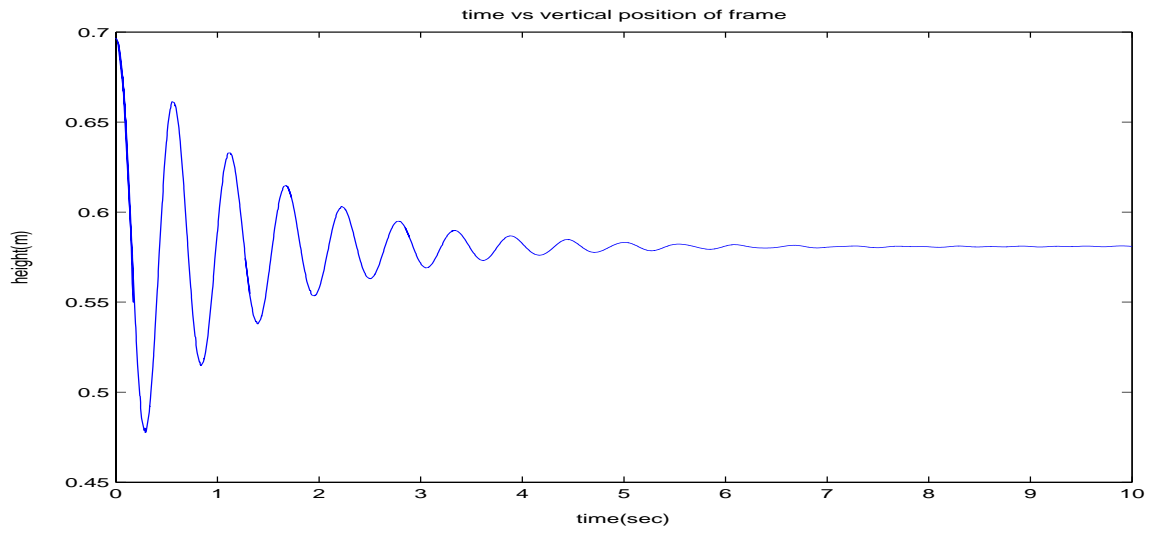


Figure 6.6: Vertical position of frame(10m/s)

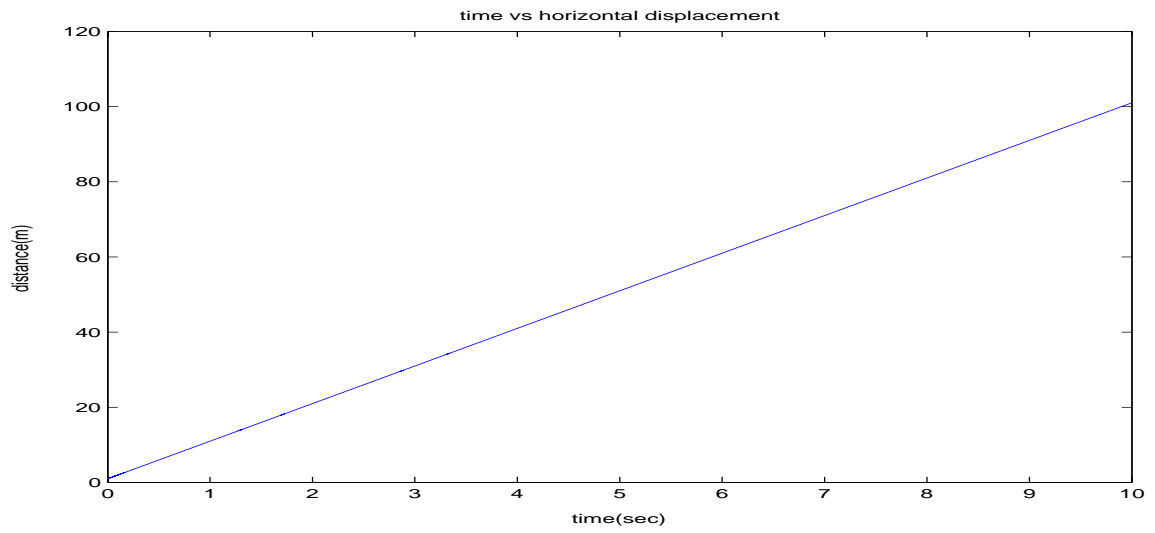


Figure 6.7: Horizontal position of axle(10m/s)

6.1.1 Conclusions

From the results of the simulations run on the vehicle model it can be seen that, 1) The frame of the vehicle comes to a steady state. 2) The trailer reaches static equilibrium. 3) All the bodies of the trailer are still attached to the vehicle. 4)The vehicle moves in a straight line. From these we can safely assume that the trailer model works.

6.2 Performance at different speeds

In this test the multibody vehicle model of the trailer is implemented along with the track model and radial springs tire model. A damping element is added at the joint connecting the axle to the walking beam, this is to be an equivalent viscous damper for friction between the bogey-axle and the walking beam . The track model is tested for two different soil conditions and three different speeds under which the trailer will normally be operated

1. The vehicle is run at slow speed (1 m/s) on sandy loam
2. The vehicle is run at medium speed (5 m/s) on sandy loam
3. The vehicle is run at high speed (10 m/s) on sandy loam
4. The vehicle is run at slow speed (1 m/s) on sand
5. The vehicle is run at medium speed (5 m/s) on sand
6. The vehicle is run at high speed (10 m/s) on sand

6.2.1 Test of track model- sandy loam

The track model is first simulated using the sandy loam as soil. The soil characteristics are published in the Theory of Ground Vehicles by J.Y.Wong. The vehicle is run at three different speeds and the response values are noted. The Vehicle is run at three different speeds, slow speed(1 m/s), medium speed(5 m/s) and high speed(10 m/s).

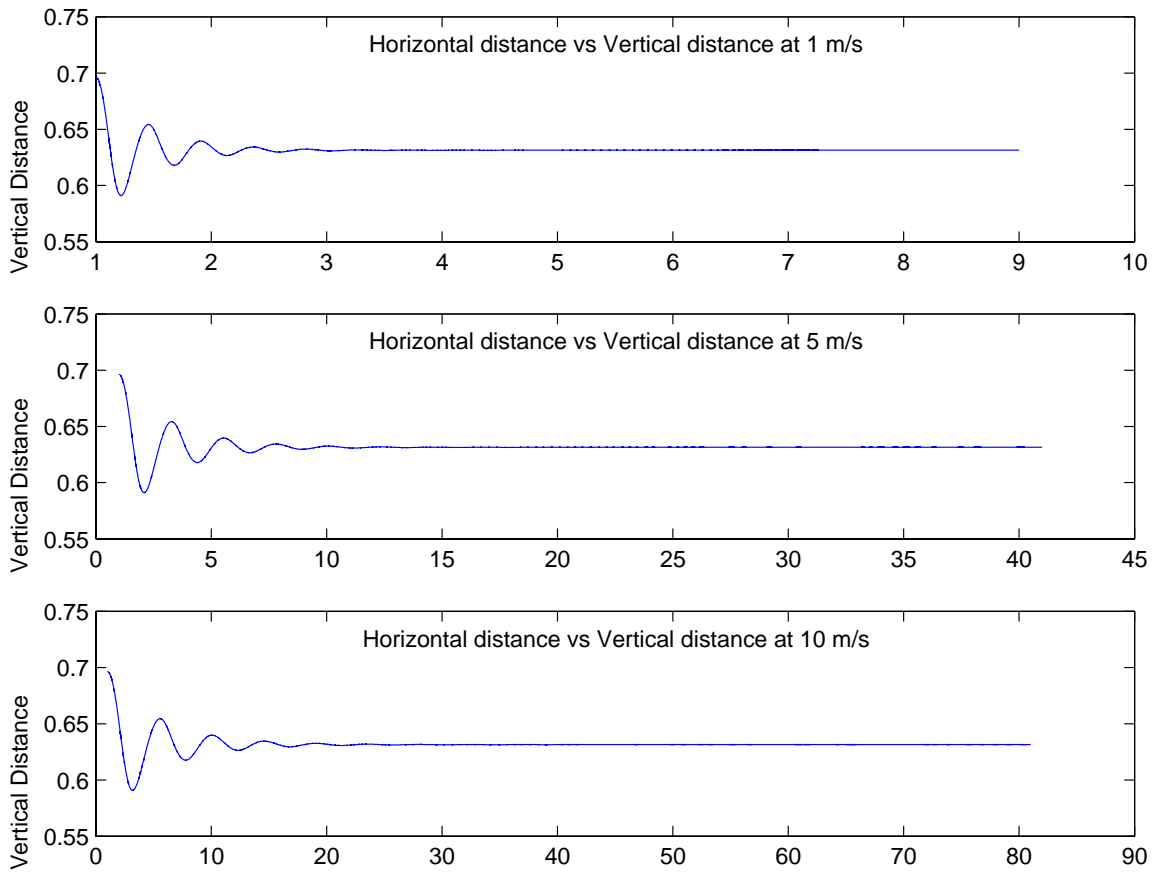


Figure 6.8: Vertical position of frame(sandy)

The Z value of the vehicle center of gravity, the angle of the walking beam, length of translation joint and the rotational velocity of the vehicle are plotted with respect to the X value of the vehicle center of gravity for each of the cases. The graphs are compared to see the effect of speed on the model.

Figure 6.8 is the Z value of the vehicles center of gravity for each of the speeds plotted against the X value of the center of gravity of the vehicle. Figure 6.10 is the angle of the walking beam for each of the speeds. Figure 6.12 and Figure 6.11 are the length of the translation joint and the rotational velocity of the vehicle for the three speeds. Figure 6.9 plots the vertical position of the walking beam and the tires.

From the test that were run on sandy loam at different speeds we can observe the

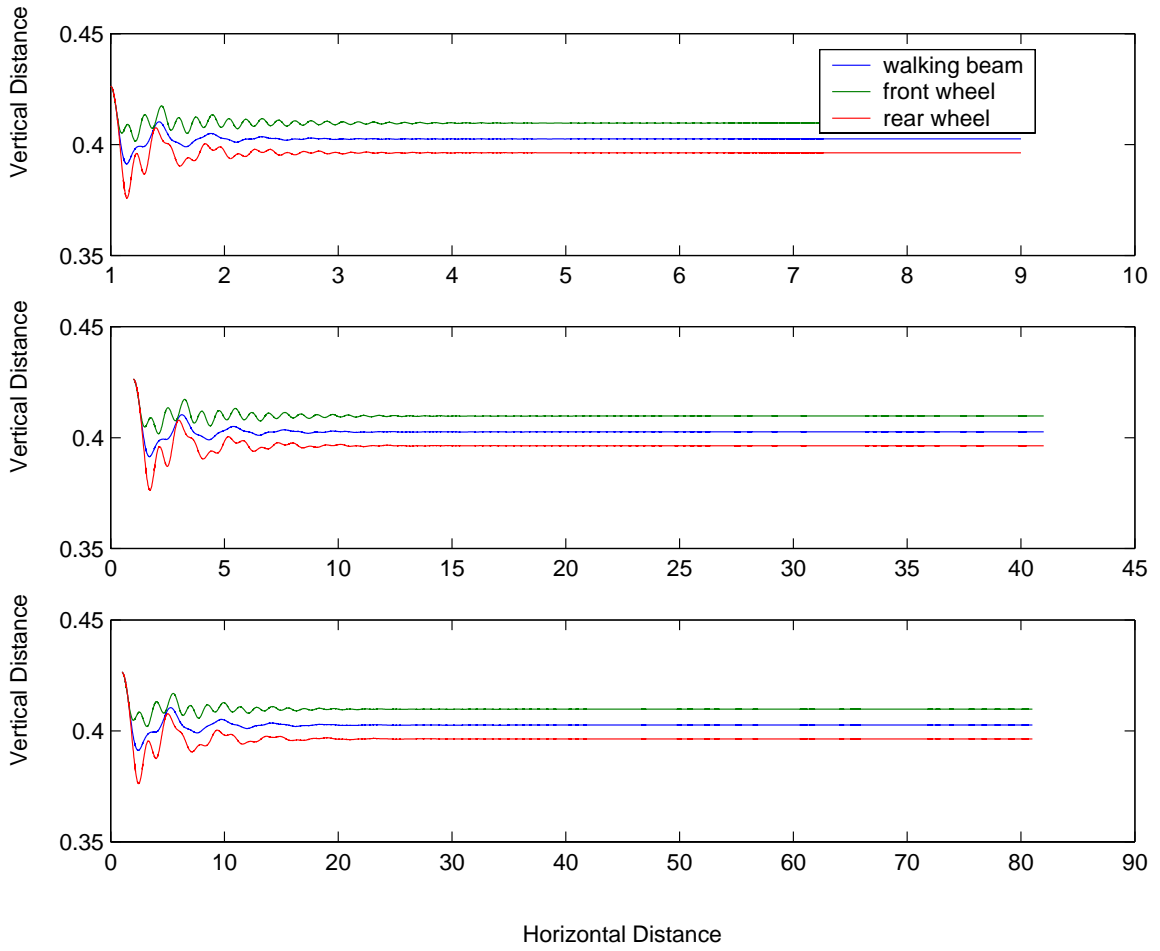


Figure 6.9: Vertical position of the walking beam and tires(sandy)

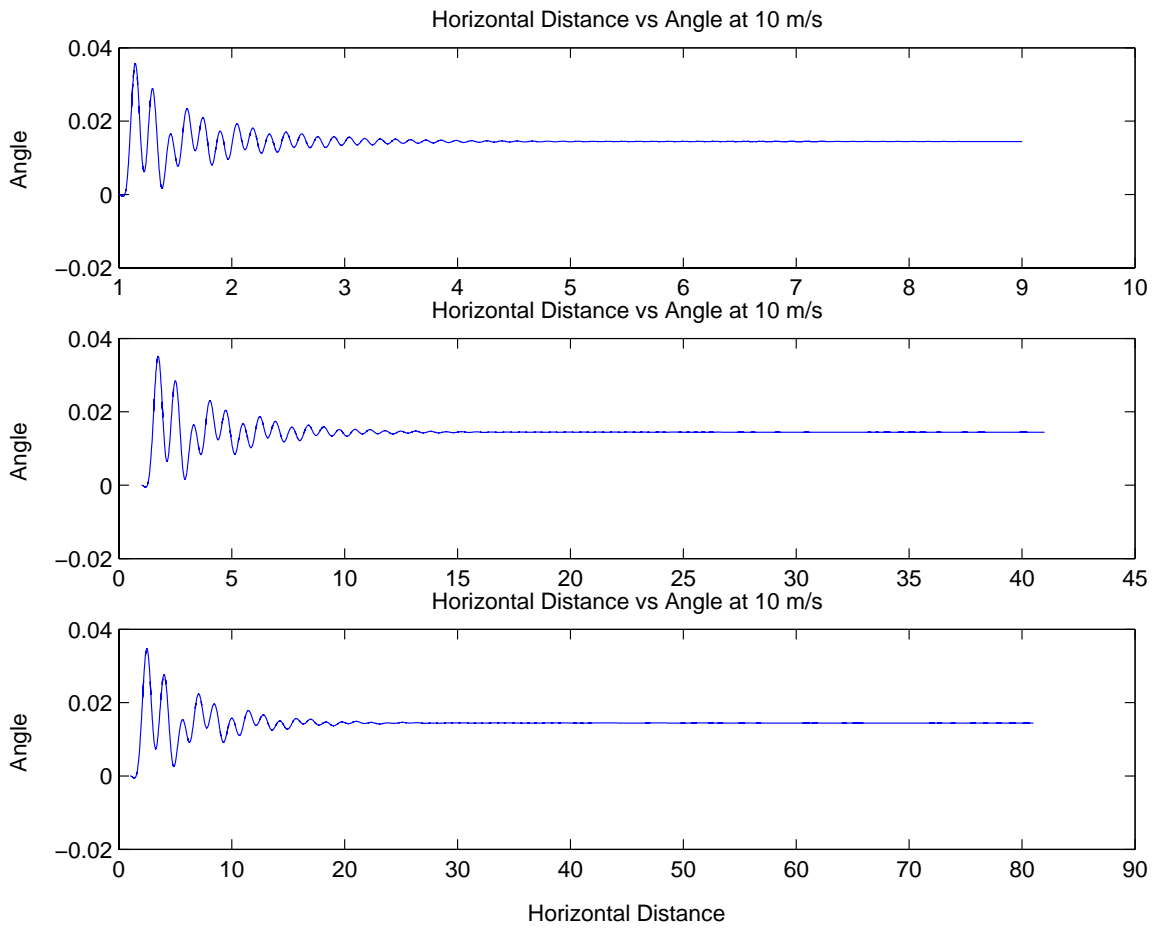


Figure 6.10: Angle of the walking beam(sandy)

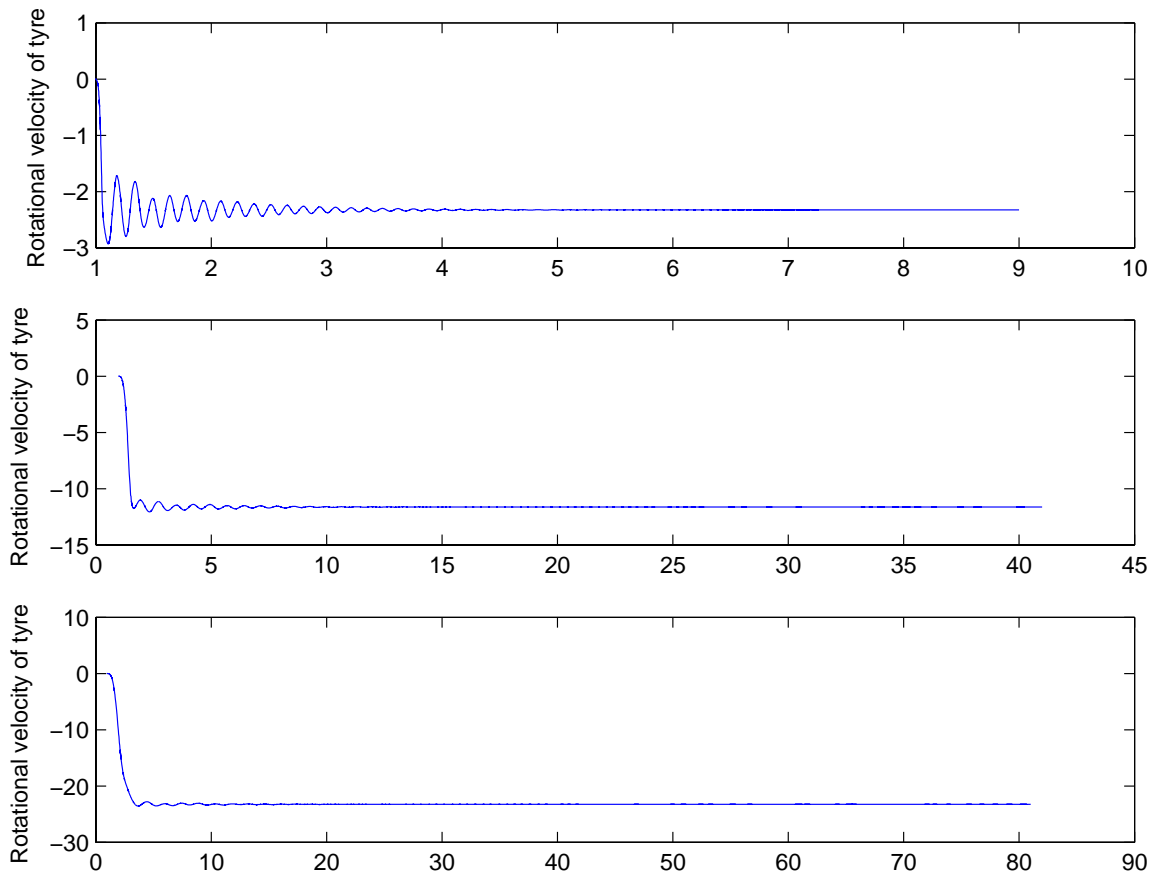


Figure 6.11: Rotaional velocity of the wheels(sandy)

Horizontal vs Rotational velocity at 1 m/s

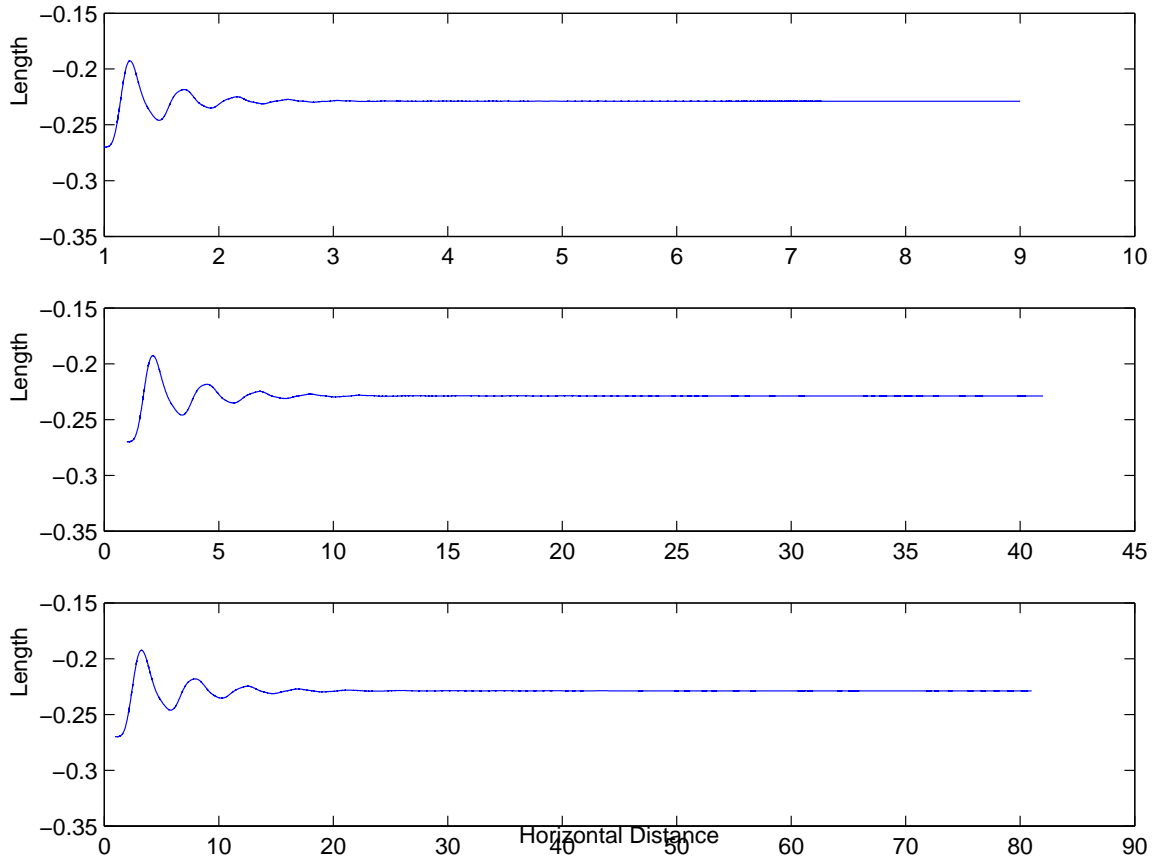


Figure 6.12: Length of translation joint(sandy)

following

1. The vehicle settles down and moves on the ground
2. From the rotational velocities of the front tires for the three different speeds, Figures 6.11, it can be noted that at steady state the slip ratio is the same.
3. From Figure 6.8 it can be seen that the vertical position of the frame remains the same at different speeds.
4. The angle of the walking beam also like the vertical position does not change at steady state.
5. Though the transient values change according to the speed, at steady state the vehicles behaves the same at different speeds.

The same results are noted when the vehicle is run over sand. The results are presented below.

6.2.2 Test of track model- sand

The track model is simulated using the sand as soil. The soil characteristics are published in the Theory of Ground Vehicles by J.Y.Wong. Just as for sandy loam the vehicle is run at three different speeds and the response values are noted. The Vehicle is run at three different speeds, slow speed(1 m/s), medium speed(5 m/s) and high speed(10 m/s). The Z value of the vehicle center of gravity, the angle of the walking beam, length of translation joint and the rotational velocity of the vehicle are plotted with respect to the X value of the vehicle center of gravity for each of the cases. The graphs are compared to see the effect of speed on the model.

Figure 6.13 is the Z value of the vehicles center of gravity for each of the speeds plotted against the X value of the center of gravity of the vehicle. Figure 6.15 is the angle of the walking beam for each of the speeds. Figure 6.17 and Figure 6.16 are the length of the translation joint and the rotational velocity of the vehicle for the three speeds. Figure 6.14 plots the vertical position of the walking beam and the tires.

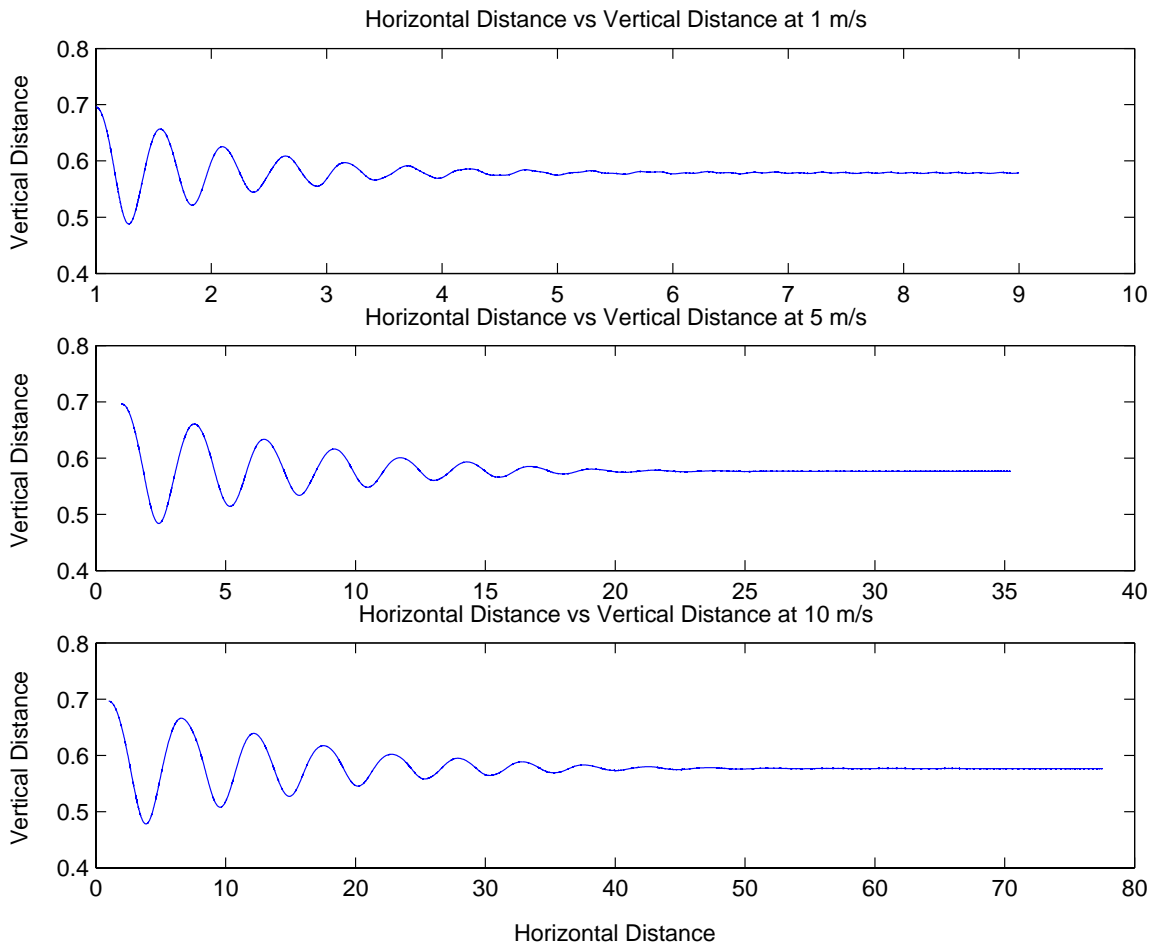


Figure 6.13: Vertical position of frame(sand)

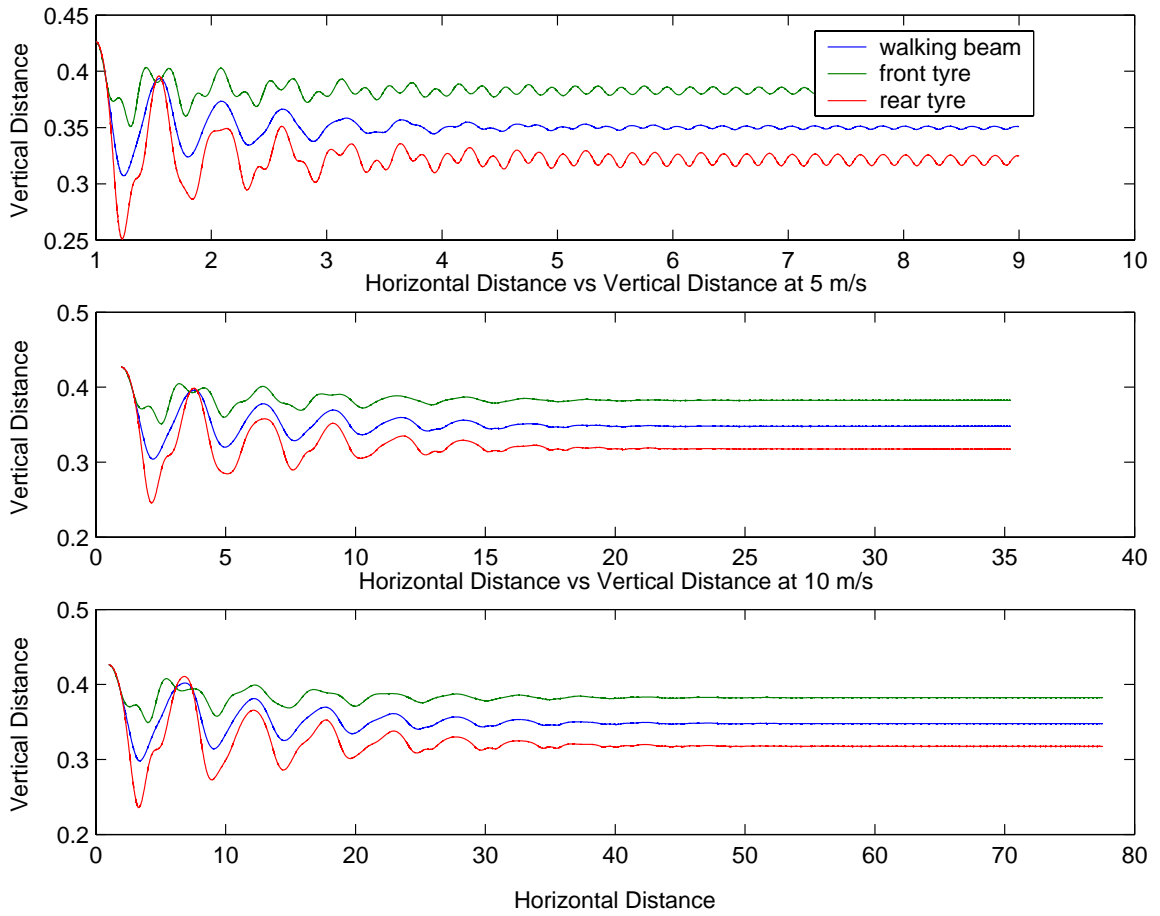


Figure 6.14: Vertical position of all bodies(sand)

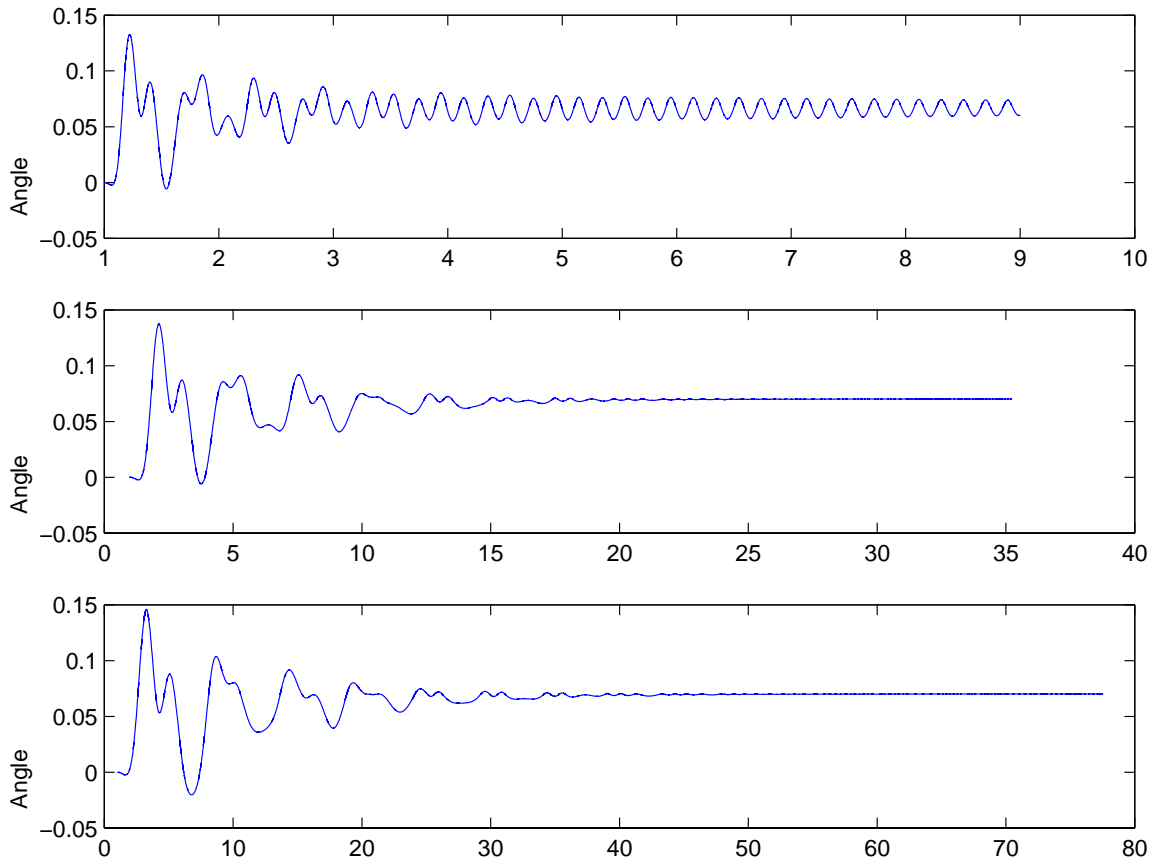


Figure 6.15: Angle of the walking beam(sand)

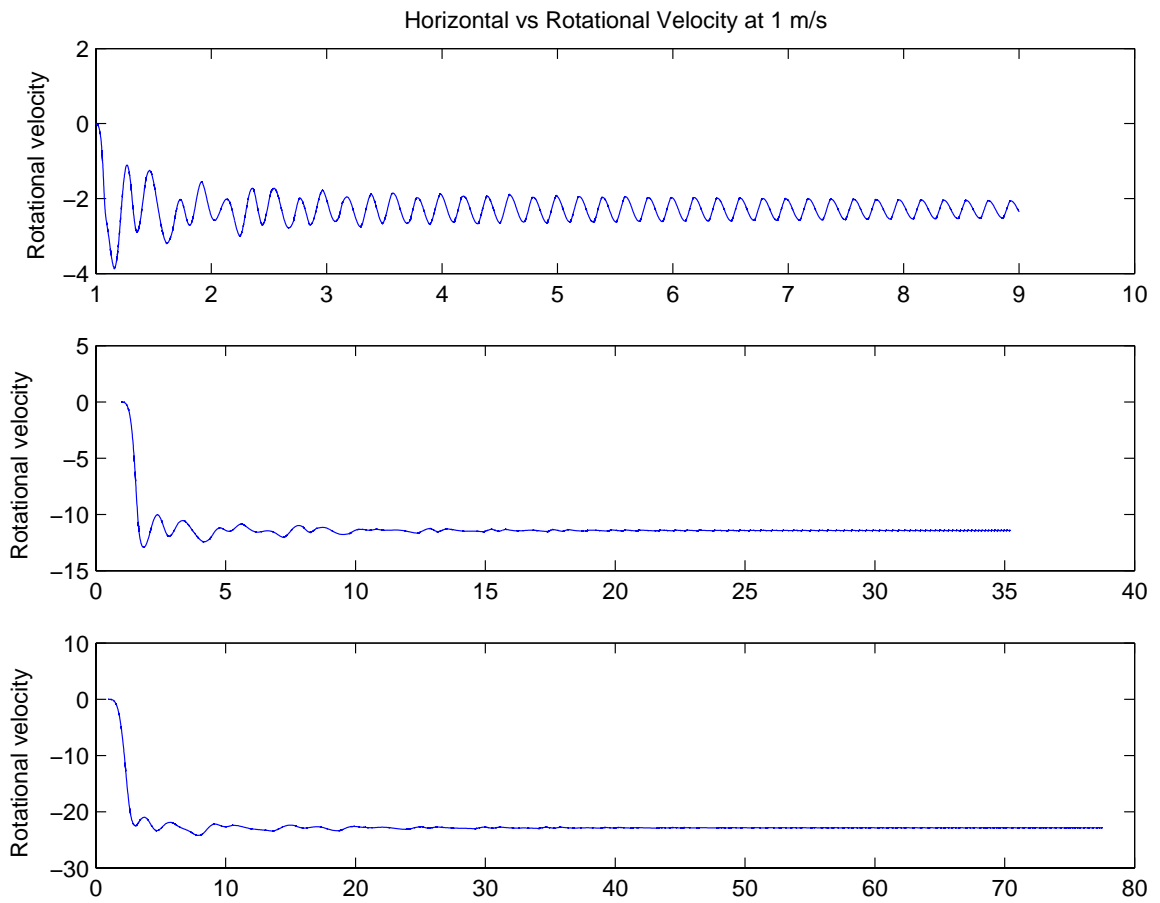


Figure 6.16: Rotaional velocity of the wheels(sand)

horizontal vs Length of translation joint at 1 m/s

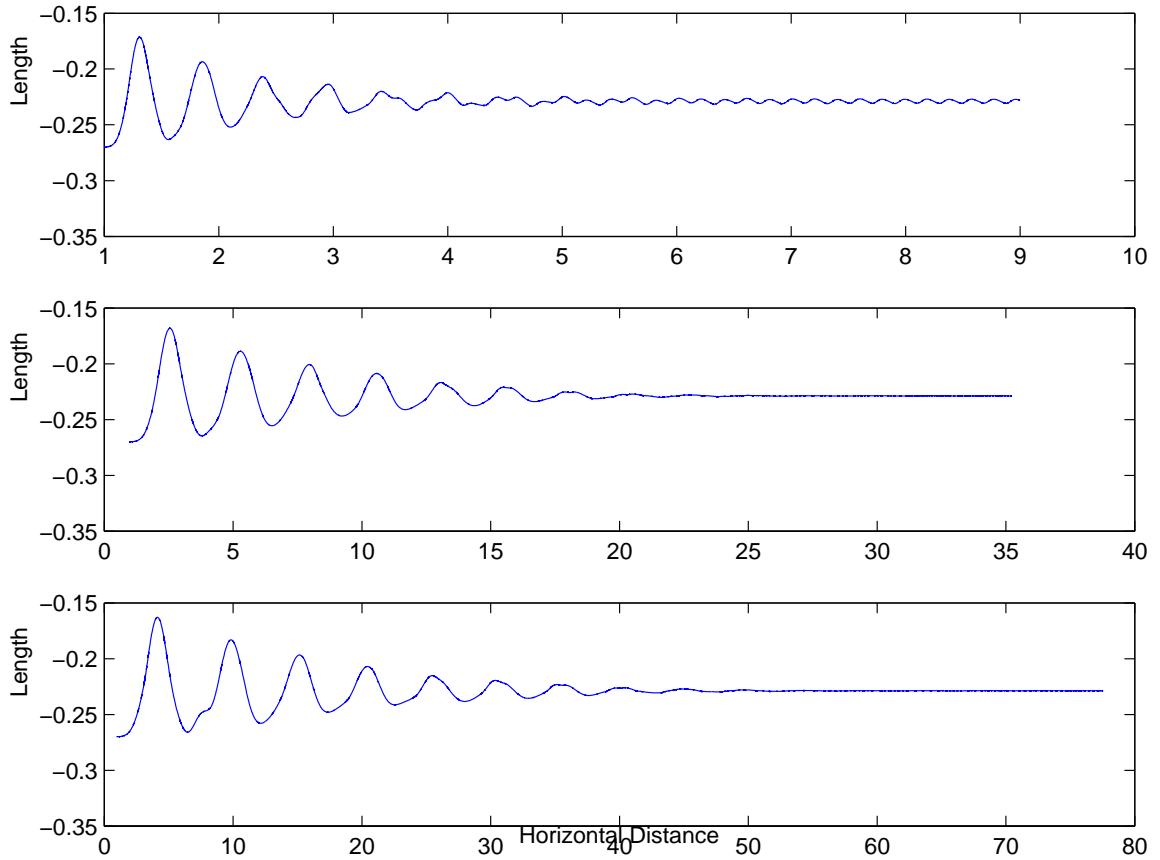


Figure 6.17: Length of translation joint(sand)

Table 6.1: Theoretical shear vs Actual shear

Slip	Shear from model	Theoretical shear
.8	44	67
1.8	311	374
9.7	553	654
14.7	815	905
20.29	973	1135
26.2	1045	1322
33.2	1301	1496

6.3 Soil performance

The vehicle is run on different soils to check the performance characteristics. The vehicle is run with different weights to check the effect of change in weight on sinkage and other parameters. The vehicle is run with different slip values to calculate the effect of slip on the shear force. The following test are run to see the effect of soil.

Figure 6.18 is the sinkage of the vehicle on three different soils. The Figures 6.20 and 6.21 are the shapes of the track when run on different soils. Figure 6.19 is the shear under the wheel. Figure 6.22 is the shear of the wheel plotted against the slip. Table 6.2 is comparative results between the theoretical sinkage and the sinkage calculated by the model. Table 6.1 is the comparative results between the theoretical shear and the shear calculated by the model. Figure 6.23 is the bar chart of the theoretical and actual shear.

1. The vehicle is run on sandy-loam, sand and clay
2. The vehicle is run with different weights
3. The vehicle is run with different slip values

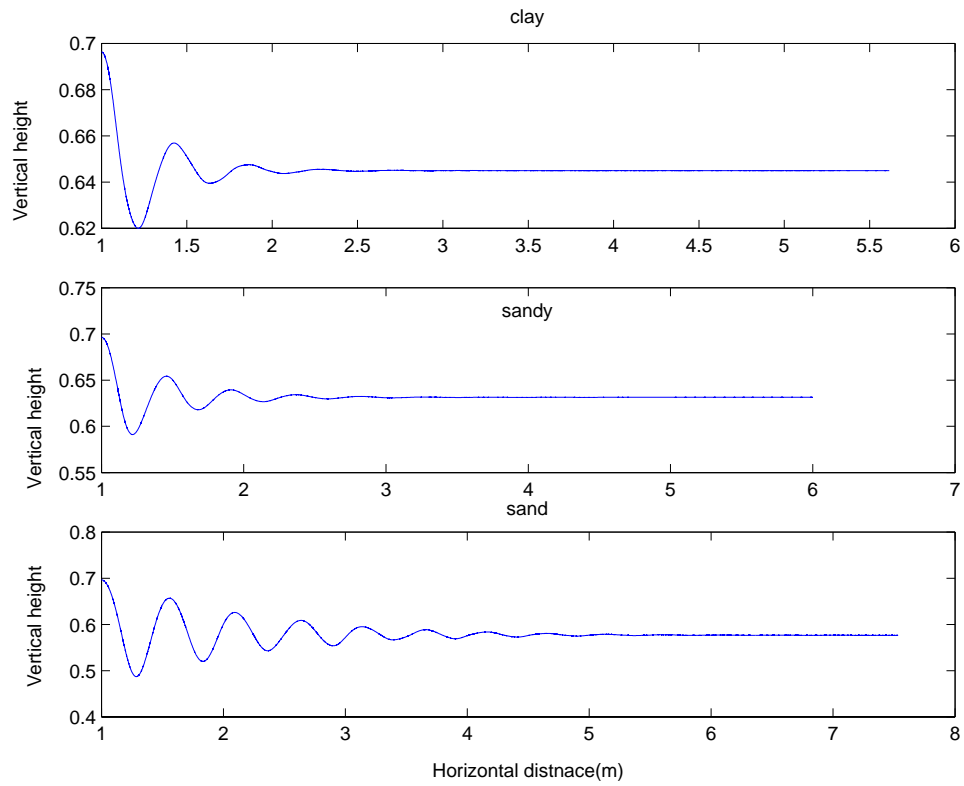


Figure 6.18: Comparative results between three different soils

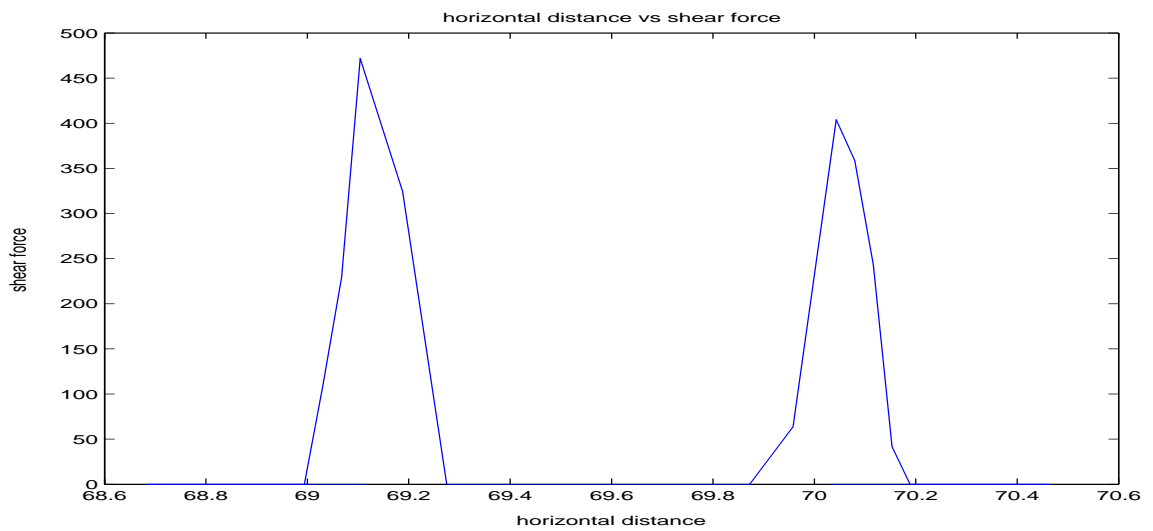


Figure 6.19: Shear force under the tires

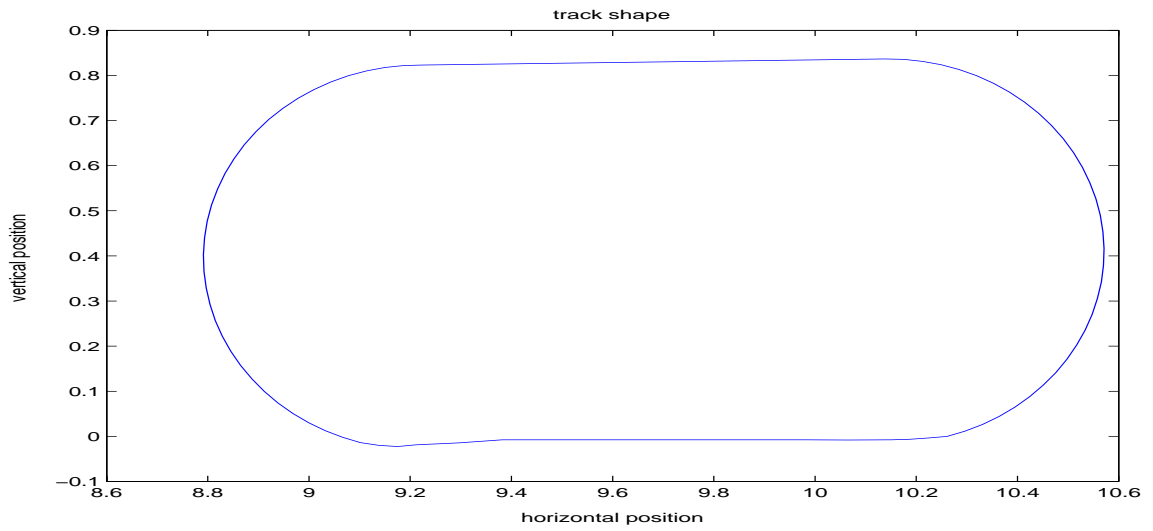


Figure 6.20: Shape of track(sandy)

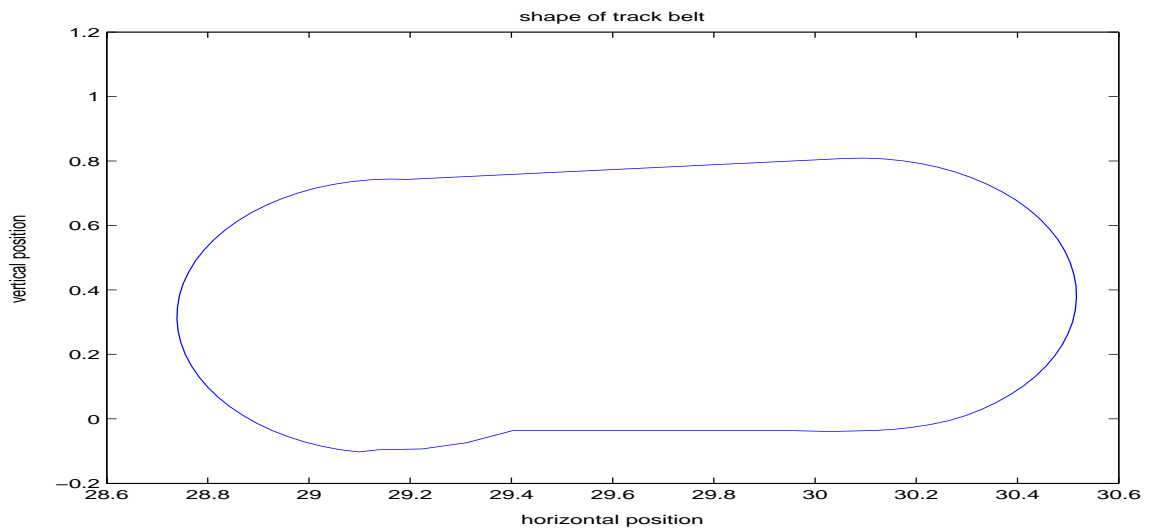


Figure 6.21: Shape of track(sand)

Table 6.2: Theoretical sinkage vs Actual sinkage

Weight (Kg)	Theoretical sinkage (m)	Actual sinkage (m)
504	.0028	.0014
554	.0030	.0015
604	.0032	.00155
654	.0033	.0016
704	.0035	.00165
754	.0037	.0017

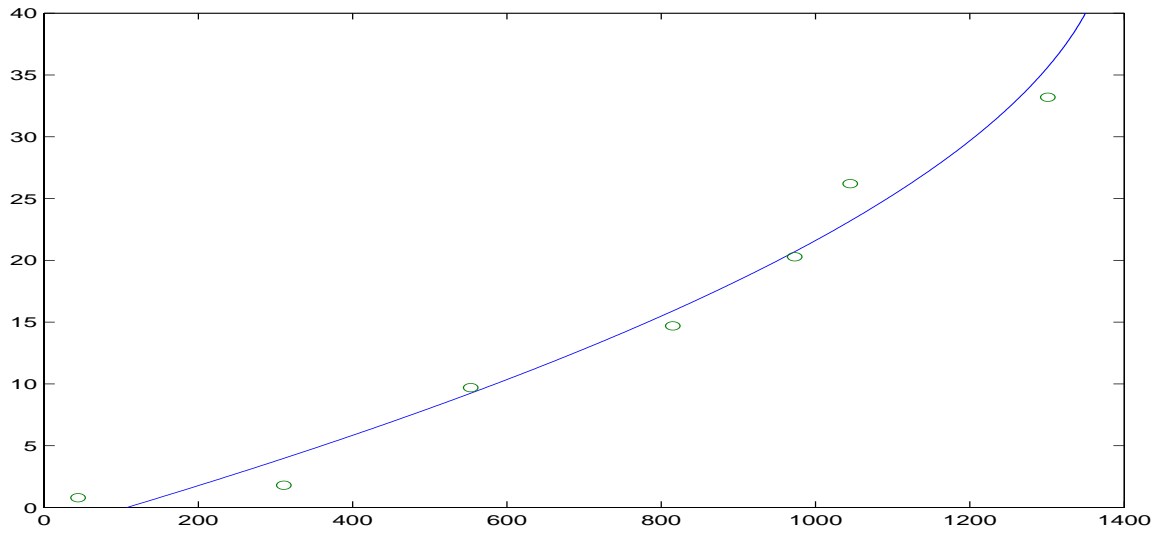


Figure 6.22: Actual shear force

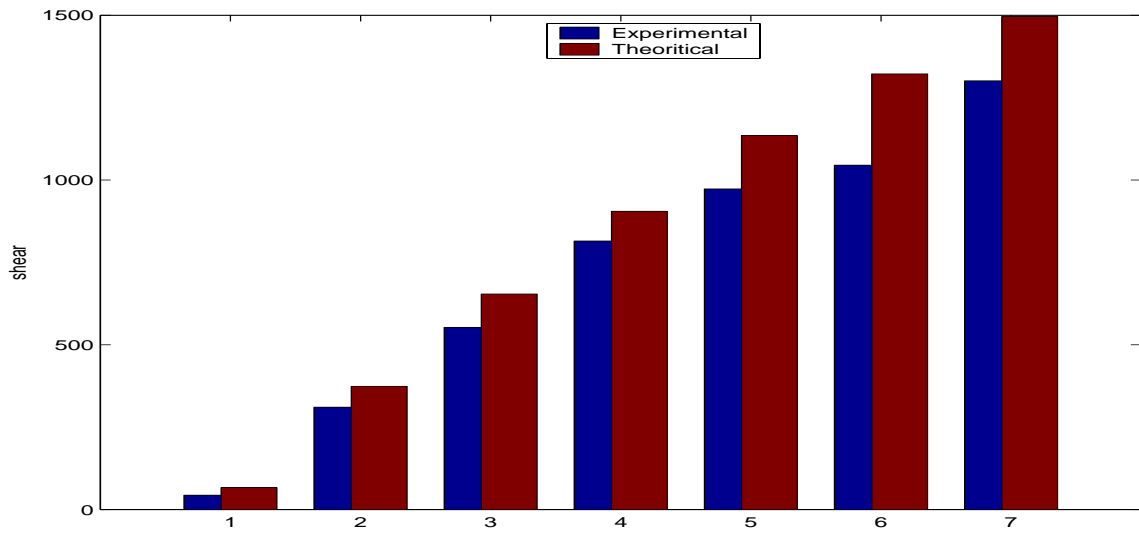


Figure 6.23: Bar graph of theoretical and actual shear

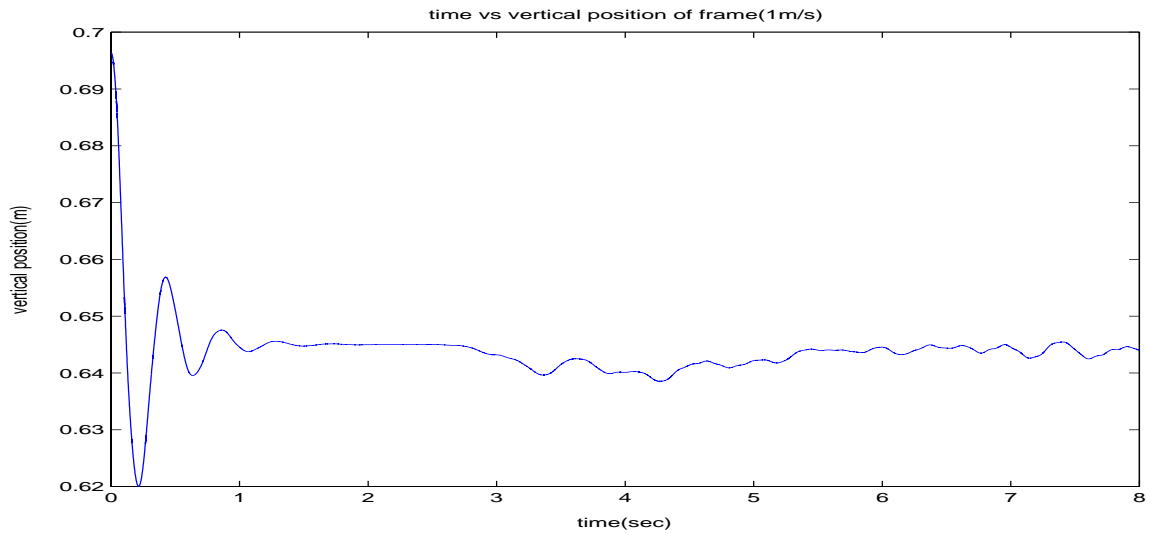


Figure 6.24: Vertical position of frame(1m/s)

6.4 Performance on rough terrain

The vehicle was run on the Belgian block course at different speeds to check the way the vehicle behaves on rough terrain.

Figures 6.24 and 6.25 are the positions of the frame when the vehicle is run at slow and high speeds over the belgian block course respectivley. Figures 6.26 and 6.27 are the plot of the vertical position of all bodies when the vehicle is run on the Belgian block course at slow and high speed respectively.

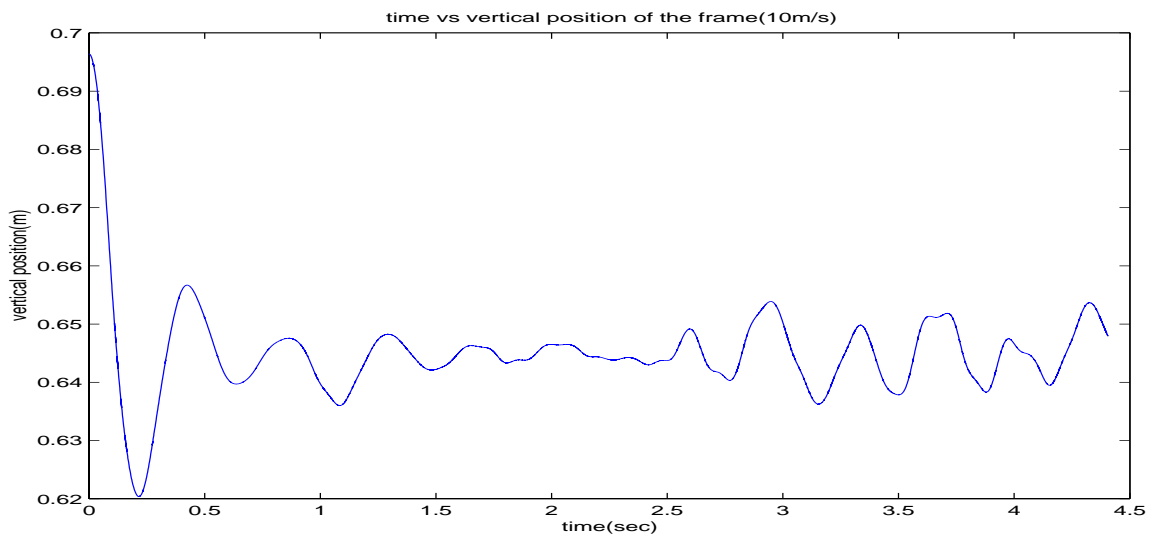


Figure 6.25: Vertical position of frame(10m/s)

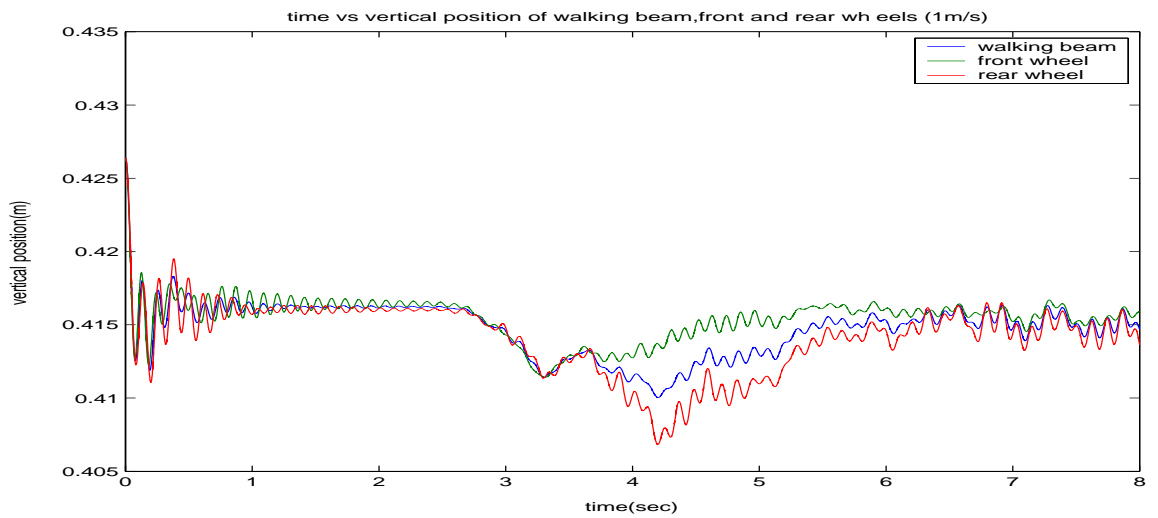


Figure 6.26: Vertical position of all bodies(1m/s)

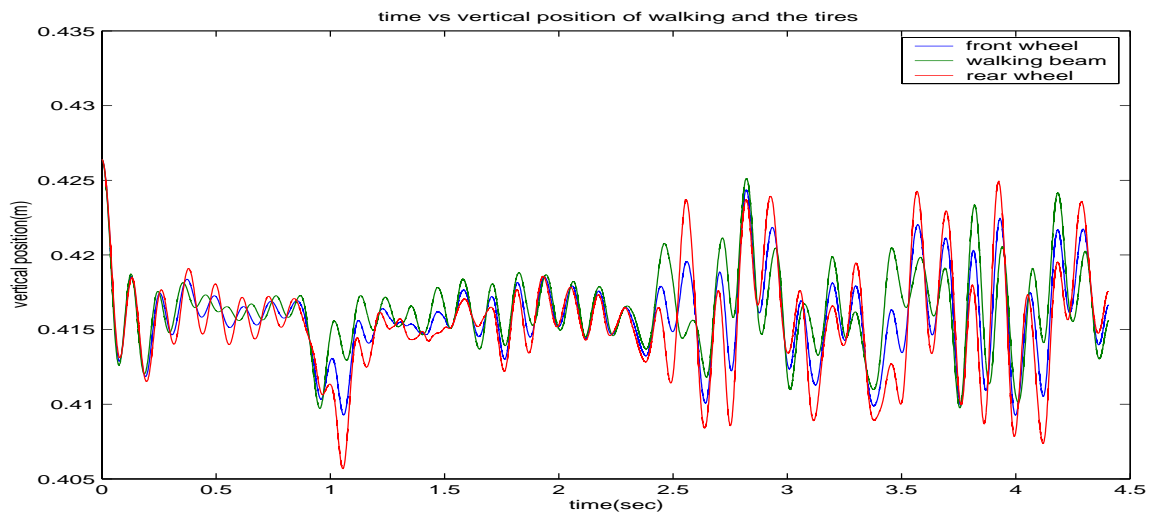


Figure 6.27: Vertical position of all bodies(10m/s)

Chapter 7

Conclusions and future work

7.1 Conclusions

This model was created to model the dynamics of a trailer with rubber band track. The thesis set out to model the dynamics of the trailer, tire and the rubber band track around the tires. This model was created for application in future durability/reliability studies.

The model for the trailer takes into account the track-terrain interaction in detail. The soil is modeled using Bekker's equations as explained in chapter 3. A multibody dynamics model was put together to model the dynamics of the trailer as explained in chapter 4. A radial spring model is used to represent the tires in this model. The rubber band track is modeled with emphasis on the track-tire and track-terrain interaction. Chapter 6 details all the test that are done and the corresponding results. The following conclusions can be drawn from the results presented.

1. The vehicle reaches steady state at all speeds and all the different soil conditions are which the model has been tested. This proves a correct and consistent behavior of the vehicle model.
2. From the positions of the wheels, it can be seen that the sinkage of the vehicle changes with respect to soil. This is consistent with the behavior that would be expected; the vehicle sinkage depends only on the soil parameters[9]. Different soils have different stiffness properties therefore the sinkage of the vehicle

changes with respect to the soil. Clay is stiffer than sandy loam which in turn is stiffer than sand, the sinkage of the vehicle follows the same pattern. The vehicle sinkage does not change with respect to the vehicle speed. This contrary to what might be expected. This phenomenon is due to the fact that the soil model does not account for soil rebound or rate of change of sinkage. The sinkage is instantaneous and therefore is not affected by the vehicle speed, for each time step regardless of the vehicle speed the sinkage values is the same.

3. It can be noted that the slip ratio for the vehicle is maintained at different speeds; the rotational velocities at steady state maintain the same slip ratio. The rate of the increase of velocity initially changes. These two trends are what would be expected, since the soil remains constant only the vehicle weight will affect the slip ration at steady state. The rate of increase will change with respect to the vehicle speed.
4. It can be seen that at steady state the angle of the walking beam changes with respect to soil and does not change with respect to the vehicle speed. In real conditions one would expect these values to change; this change is not noted in the simulations due to the fact that the soil model does not account for any rebound. The vehicle sinkage is instantaneous, therefore does not change with respect to speed, only changes with respect to the weight of the vehicle and the soil.
5. It can be seen that the front wheel is always situated above the rear wheel This due to the fact that the soil is plastic and therefore as the front wheels rolls over the soil it flattens the ground and the ground level is assumed to be the lowest point of the front wheel. It can also be seen that the track follows the tire profile and the track between wheels also follows the expected path.
6. The vehicle is unable to simulate correctly the mean maximum ground pressure due to the fact that in the model there is no sinkage between the wheels. This is due to the fact that there is no bending stiffness in the tracks and therefore

the track is assumed to lie flat on the ground.

7. The shear forces for different slips and the sinkage for different weights are tabulated. These values are compared to the theoretical values. The theoretical values are calculated for a flat plate of area $0.12m^2$. The values match quite well. All the values are within the limits one might expect. There is a significant difference between the theoretical and actual sinkages. This is due to the fact that the actual sinkage takes into account the deflection of the tires and the fact that theoretical values are meant for a flat rectangular plate.
8. Figure represent the plot of shear with respect to the slip. The curve is similar to other curves generated by studies done by Dr. J. Y. Wong[7]

From all the above test we can conclude that the track model functions well on different soil at different speeds. The model also is able to simulate the vehicle moving on the Belgian block course.

From the results of the simulations conducted it can be concluded that this model is suitable for use in future durability/reliability studies. The models deficiencies are primarily due to the lack of a good soil model. The model can be improved by adding bending stress to the track. The parameters of the model like the number of elements, stiffness etc can be modified. The tire and track forces are calculated accurately. This model further can be used as a test bed for improving the soil model. The rate of sinkage could be added as a parameter to the soil model. The results of the simulations could be used to calculate the rate of sinkage of the soil.

7.2 Future work

This model works effectively for straight line testing on different soils. The data computed from the simulations have not been verified due to the unavailability of test data on the vehicle. The model has only been verified. There are many limitations to this model. The model does not accurately predict the Mean Maximum Ground pressure due to the fact that the track does not have any bending stiffness. Due to

this the track between the wheels is assumed to have no sinkage at all, therefore not contributing to soil resistance to sinkage. Due to the limitations of the soil model the sinkage of the vehicle at all speeds is the same. In this model the upper part of the track is not modeled, it is assumed that the upper part of the track just deflects to take care of the extra tension developed when the vehicle starts moving. The upper part of the track has to be modeled accurately to increase the accuracy of the model. This model also does not work when the vehicle is turned, the lateral forces are not calculated in the model. The model can be improved in the following ways.

1. Due to the fact that there is no available test data for the particular trailer, the model was not verified. To improve the model and change some of the parameters the results got from the simulation have to be compared with test data.
2. Addition of bending stiffness to the model is an important step to increase the accuracy of the model. This in turn will help predict the effect of the trailer running over large bumps as well as improve the prediction of the mean maximum ground pressure.
3. An accurate model of the soil; which includes rebound and rate of sinkage, has to be developed. This model will in turn help in predicting the sinkage characteristics better. The rate of sinkage of the soil will help in modeling the effect of speed on the trailer.
4. Develop a model to describe the upper portion of the track to improve the connectivity algorithm and acquire a more complete picture of the tension in the track.

BIBLIOGRAPHY

Bibliography

- [1] Nads vehicle dynamics software release 4. Technical report, University of Iowa, 1994.
- [2] S.Sankar A.Dhir. Dynamics of off-road tracked vehicles equipped with trailing arm suspension. *Proceedings of the Institution of Mechanical Engineers*, 209:397–411, 1995.
- [3] corina sandu. *Tracked Vehicle Modeling*. PhD thesis, University of Iowa, Iowa city, Iowa, 2000.
- [4] Jeffrey Freeman Dan negrut. Dynamic tire modelling for application with vehicle simulations incorporating terrain. *Society Of automotive engineers*, 1994.
- [5] Roberto Girelli Gianni Ferreti. Modelling and simulation of an agricultural tracked vehicle. *Journal of Terramechanics*, 36:139–158, 1999.
- [6] G.R.Doyle J.M.Badalamenti. Radia-interradial spring tire models. *American Society of Mechanical Engineers*, 110:70–75, 1995.
- [7] J.Y.Wong. *Theory of Ground Vehicles*. Wiley interscience, 1978.
- [8] J.Y.Wong. An introduction to terramechanics. *Journal of Terramechanics*, 21:5–17, 1984.
- [9] M.G.Bekker. *Introduction to Terrain Vehicle Systems*. The university of Michigan Press, 1969.

- [10] A.A.Shabana M.K.Sarwar, Toshikazu Nakanishi. Chain link deformation in the nonlinear dynamics of tracked vehicles. *Journal of Vibration and Control*, 1:201–224, 1995.
- [11] M.Saarilahti. Soil interaction model. Technical report, Department of forest resource management, University of Helsinki, 2002.
- [12] A.A.Shabana T.Nakanishi. On the numerical solutions of tracked vehicle dynamic equation. *Nonlinear Dynamics*, 6:391–417, 1994.

Vita

Vita

Hemmant Gopal was born in Madras, India. He got his Bachelor of Engineering Degree from the University of Madras in the field of Automobile engineering. He got his Master of Science degree from the University of Tennessee, Knoxville in the field of Mechanical Engineering.